COP9 signalosome component CSN-5 stabilizes PUF proteins FBF-1 and FBF-2 in *Caenorhabditis elegans* germline stem cells

Short title: CSN-5 stabilizes FBF-1/-2 in stem cells

Emily Osterli, Mary Ellenbecker, Xiaobo Wang[1], Mikaya Terzo, Ketch Jacobson, DeAnna Cuello, Ekaterina Voronina*

Division of Biological Sciences, University of Montana, Missoula, MT, 59812, USA

[1]current address: Dermatology Hospital, Southern Medical University, Guangzhou, China

*Corresponding author: ekaterina.voronina@umontana.edu

Abstract:

RNA-binding proteins FBF-1 and FBF-2 (FBFs) are required for germline stem cell maintenance and the sperm/oocyte switch in *Caenorhabditis elegans*, though the mechanisms controlling FBF protein levels remain unknown. We identified an interaction between both FBFs and CSN-5, a component of the COP9 (constitutive photomorphogenesis 9) signalosome. Here, we find that the MPN (Mpr1/Pad1 N-terminal) metalloprotease domain of CSN-5 interacts with the PUF (Pumilio and FBF) RNA-binding domain of FBFs and the interaction is conserved for human homologs PUM1 and CSN5. The interaction between FBF-2 and CSN-5 can be detected *in vivo* by proximity ligation. *csn-5* mutation results in destabilization of FBF proteins, a decrease in the numbers of germline stem cells, and disruption of the switch from spermatogenesis to oogenesis. The loss of *csn-5* does not decrease the levels of a related PUF protein PUF-3 and *csn-5(lf*) phenotype is not enhanced by *fbf-1/2* depletion, suggesting that the effect is specific to FBFs. The effect of *csn-5* on germline sex determination is largely independent of the COP9 signalosome and is cell autonomous. Surprisingly, regulation of FBF protein levels involves a combination of COP9-dependent and –independent mechanisms differentially affecting FBF-1 and FBF-2. This work supports a previously unappreciated role for CSN-5 in stabilization of germline stem cell regulatory proteins FBF-1 and FBF-2.

Author Summary:

Germ cell development and reproductive success in the nematode *C. elegans* rely on the function of germline stem cells. Continued maintenance of these cells is supported by the activity of conserved RNA-binding proteins FBF-1 and FBF-2 (FBFs). However, it is unknown how FBF protein levels are regulated. Here, we identify a direct interaction between FBFs and CSN-5, a component of the COP9 signalosome best known for its role in regulating protein degradation. We find that CSN-5 promotes FBF stability and allows for accumulation of steady-state protein levels, thereby promoting FBF function. In *csn-5* mutants, we find a significant reduction of FBF proteins, decrease of stem cells,

and failure to promote oogenesis consistent with compromised FBF function. Furthermore, CSN-5 contributes to FBF protein stability through two mechanisms. This work demonstrates a previously unappreciated role for CSN-5 in stabilization of FBF proteins. Based on our finding that the FBF/CSN-5 interaction is conserved and detectable between homologous human proteins, we speculate this relationship might be relevant for understanding stem cell maintenance in a range of species, from nematodes to humans.

Introduction:

Stem cells are a population of unspecialized cells with the capability to both self-renew and preserve the stem cell pool or to differentiate and support tissue maintenance (Morrison and Kimble, 2006). Stem cell function depends on faithful expression of essential developmental regulators (Morrison et al., 1997). A number of mechanisms controlling expression of stem cell machinery at the levels of epigenetics, transcription, and RNA stability have been widely studied (for example, Lee et al., 2016; Chen et al., 2020; Samuels et al., 2020; Demarco et al., 2022; Vogiatzoglou et al., 2022). As the stem cell proteome is exquisitely controlled in both self-renewing state and through developmental transitions (Vilchez et al., 2014; Llamas et al., 2020), it is critical to understand the mechanisms regulating stability of key self-renewal factors.

We use the *C. elegans* germline to study stem cell regulators FBF-1 and FBF-2 (FBFs). The *C. elegans* gonad consists of two U-shaped arms, each with a population of stem and progenitor cells (SPCs) at the distal end (Fig. 1A; Kimble and White, 1981). SPCs are maintained through the GLP-1/Notch signaling from the somatic niche cell (Austin and Kimble, 1987; Berry et al., 1997; Kimble and Crittenden, 2007). As the cells progress away from the niche, they begin to differentiate and enter meiosis before generating gametes at the proximal end (Hubbard, 2007; Pazdernik and Schedl, 2013; Voronina and Greenstein, 2016). The hermaphrodite germlines produce sperm during larval development and switch to oogenesis in the young adults (Pazdernik and Schedl, 2013).

76 FBFs are RNA-binding proteins belonging to the highly conserved PUF (Pumilio and
77 FBF) family (Wickens et al., 2002). FBFs are enriched in SPCs (Fig. 1A) and act by
78 binding to and repressing their target mRNAs (Zhang et al., 1997; Crittenden et al.,
79 2002; Prasad et al., 2016). FBFs promote germline stem cell maintenance, and *fbf-1 fbf-*
80 *2* double mutant germline stem cells prematurely enter meiosis during late larval
81 development (Crittenden et al., 2002; Wickens et al., 2002; Wang and Voronina, 2020).
82 Consistent with this function, many FBF targets encode developmental regulators,
83 which are silenced in stem cells and then activated upon differentiation, such as the
84 differentiation-promoting protein GLD-1 (Crittenden et al., 2002; Suh et al., 2009). FBFs
85 also promote self-renewal of germline stem cells by repressing *cki-2* (Kalchhauser et al.,
86 2011), a Cyclin E/Cdk2 inhibitor which regulates the decision to enter/exit the cell cycle
87 (Buck et al., 2009). Additionally, FBF-1 and FBF-2 regulate germline sex determination
88 by facilitating the switch from spermatogenesis to oogenesis (Zhang et al., 1997) as *fbf-*
89 *1 fbf-2* double mutant gonads fail to undergo oogenesis, resulting in a masculinization of
90 germline (Mog) phenotype where only sperm is produced (Crittenden et al., 2002).
91 Despite these well-characterized functions of FBFs, the post-translational mechanisms
92 regulating the levels of FBF proteins in stem cells remain unknown.

93 One prominent cellular mechanism impacting protein stability and steady-state levels
94 involves the COP9 (constitutive photomorphogenesis 9) signalosome, a highly
95 conserved enzymatic complex composed of eight subunits, denoted CSN1 to CSN8
96 (Qin et al., 2020). Although initially discovered for its role in regulation of transcription
97 (Wei and Deng, 1992), the COP9 signalosome's best documented function is as a
98 regulator of protein degradation (Wei et al., 1994; Chamovitz et al., 1996; Claret et al.,
99 1996; Chamovitz, 2009). COP9 impacts protein degradation by removing a ubiquitin-like
100 protein, NEDD8, from cullin subunits of E3 ubiquitin ligases (Cope et al., 2002;
101 Lingaraju et al., 2014). The balance between neddylation and deneddylation is essential
102 to maintain the activity of cullin-based ubiquitin ligases and to facilitate the degradation
103 of their substrates (Lyapina et al., 2001; Doronkin et al., 2003; Pintard et al., 2003; Wu
104 et al., 2005). The overall architecture of COP9 resembles the 19S lid of the 26S
105 proteasome, which is responsible for the majority of intracellular protein degradation
106 (Enchev et al., 2012; Lingaraju et al., 2014). CSN subunits 1-4, 7, and 8 contain PCI

107 (**P**roteasome, **C**OP9 signalosome, translation **I**nitiation factor) domains similar to the six
108 subunits of the proteasome lid (Dessau et al., 2008; Hofmann and Bucher, 1998). COP9
109 signalosome subunit 5 (CSN5) is the only catalytically competent component and
110 contains a JAB1/MPN (**M**pr1/**P**ad1 **N**-terminal) metalloprotease domain, which is
111 responsible for the complex's deneddylating activity (Zhang et al., 2012; Echalier et al.,
112 2013). The signalosome is inactive without the incorporation of CSN5, and likewise, the
113 current literature suggests CSN5 is inactive on its own and unable to deneddylate
114 cullins in isolation (Cope et al., 2002; Sharon et al., 2009; Echalier et al., 2013;
115 Lingaraju et al., 2014). Furthermore, CSN5 must dimerize with the other MPN domain-
116 containing COP9 subunit CSN6, to be incorporated into the COP9 holoenzyme and
117 become activated (Birol et al., 2014; Lingaraju et al., 2014). Apart from COP9 subunits,
118 CSN5 has been reported to interact with other cellular proteins (Tomoda et al., 1999;
119 Smith et al., 2002; Yoshida et al., 2013; Shackleford and Claret, 2010) and to promote
120 accumulation of several of its partners (Bae et al., 2002; Bemis et al., 2004; Orsborn et
121 al., 2007; Liu et al., 2009; Lim et al., 2016). Furthermore, CSN5 interaction partners may
122 be stabilized in a manner dependent on the entire COP9 complex (Wu et al., 2009) or
123 independently of the COP9 holoenzyme (Bemis et al., 2004).

124 In a yeast-two hybrid screen for FBF binding partners, we identified *C. elegans* CSN-5
125 as an interactor of FBF-2. This work investigates CSN-5's contribution to FBF function
126 in the germline. We find that CSN-5 stabilizes both FBF-1 and FBF-2 in germline SPCs,
127 correlating with effective stem cell maintenance and female fate. Our findings identify a
128 previously unappreciated role for CSN-5 and we speculate its contribution to stem cell
129 regulatory protein accumulation is relevant to a wide range of organisms.

130

131 **Results:**

132 **CSN-5 is a new interacting partner of FBFs**

133 To identify proteins that associate with FBF-2, we performed a yeast two-hybrid screen
134 of a *C. elegans* cDNA library with FBF-2 as bait (see Materials and Methods for detail).
135 Briefly, the yeast transformed with full-length FBF-2 fused to the Gal4 DNA-binding

domain were mated to a yeast library of mixed-stage wild type *C. elegans* cDNAs fused to the Gal4 activation domain. Resulting diploids were selected for growth on minimal media lacking histidine and adenine selecting for expression of *HIS3* and *ADE2*, with the addition of 1 mM 3-AT (a competitive inhibitor of the HIS3 enzyme) added for stringency. The screen of estimated $2x10^8$ yeast diploids identified a known FBF interactor SYGL-1 (Shin et al., 2017) as well as several potential new interactors (Table S1), with one of the most abundant partners representing a fragment of COP9 signalosome subunit CSN-5. To validate this potential interaction and to test whether CSN-5 might bind FBF-1 as well as FBF-2, we performed a directed yeast two-hybrid assay, in which full-length FBF-1 or FBF-2 fused to the Gal4 DNA-binding domain were cotransformed with full-length CSN-5 fused to the Gal4 activation domain. Robust growth was observed when CSN-5 was co-transformed with either FBF-1 or FBF-2, but not in controls (Fig. 1B). Yeast expression of c-myc-tagged FBFs and HA-tagged CSN-5 was detected by Western blot using anti-Myc and anti-HA, respectively (Fig. 1C). We conclude that CSN-5 interacts with both FBF-1 and FBF-2 in yeast. Additionally, we performed a GST pulldown assay with bacterially-expressed GST-tagged CSN-5 and His_6-tagged FBFs, which detected direct interaction between these proteins (Fig. 1D).

The interaction between the RNA-binding domain of FBFs and the MPN domain of CSN-5 is conserved in evolution

To elucidate the location of the interacting domains within FBFs and CSN-5, we generated several truncation constructs of FBF-1, FBF-2, and CSN-5 expressing distinct domains amenable to recombinant expression based on the previous studies (Fig. 2B, D; Bernstein et al., 2005; Echalier et al., 2013; Birol et al., 2014), and tested their association via GST pulldown assay. We observed that the conserved RNA-binding domains (RBDs) of both FBFs were sufficient for the interaction with CSN-5, and the binding between FBF-2 and CSN-5 was lost in the absence of FBF-2 RBD (Fig. 2A). Furthermore, the interaction between FBF-2 and CSN-5 was dependent on CSN-5^{MPN} domain (Fig. 2C). We then tested whether FBF-2 could interact with the other MPN domain of COP9 signalosome, contributed by CSN-6. The MPN domain of CSN-6 was delineated by homology to human CSN6 (Ma et al., 2014). GST pulldown assay

166 suggested that the interaction of His_6::FBF-2 with GST::CSN-6^{MPN} is much weaker than
167 that with CSN-5^{MPN} (Fig. 2E). We concluded that the FBF/CSN-5 interaction is mediated
168 by the conserved, structured domains, with selectivity towards specific members of the
169 domain families. We further tested whether FBF-2 interaction with MPN domains of
170 CSN-5 and CSN-6 was RNA-dependent, and found that the binding was not disrupted
171 by the RNase A treatment (Fig. S1).

172 Both FBFs and CSN-5 have homologous human proteins, PUM1/PUM2 and CSN5,
173 respectively (Spassov and Jurecic, 2002; Qin et al., 2020). We tested whether the
174 RBDs and MPN domain of the corresponding human homologs (Fig. 2B, D) were able
175 to interact. A GST pulldown assay of GST::$CSN5^{MPN}$ with His_6::$PUM1^{RBD}$ and
176 His_6::$PUM2^{RBD}$ revealed that the interaction we observed for the nematode proteins is
177 conserved for human homologs CSN5 and PUM1, but not PUM2, suggesting an
178 evolutionarily conserved protein complex (Fig. 2F). We considered whether CSN-5 were
179 able to interact with other *C. elegans* PUF proteins including PUF-8, PUF-11, and PUF-
180 3, but were unable to produce soluble recombinant PUF proteins to test this hypothesis.

181

182 **FBF-2 interacts with CSN-5 *in vivo***

183 After characterizing the interaction between FBFs and CSN-5 *in vitro*, we tested if this
184 interaction is also observed *in vivo*. We utilized proximity ligation assays (PLA) to detect
185 *in situ* protein-protein interactions at distances <40 nm (Söderberg et al., 2008; Day et
186 al., 2020). PLA was performed on *3xflag::csn-5; gfp::fbf-1* and *3xflag::csn-5; gfp::fbf-2*
187 animals using *3xflag::csn-5; gfp* as a control for spurious proximity. We observed a
188 statistically significant (p<0.0001; Fig. 3) increase in PLA signal within the SPC zone in
189 *3xflag::csn-5; gfp::fbf-2* compared to both control and *3xflag::csn-5; gfp::fbf-1.* Curiously,
190 there was no significant difference in PLA signal between *3xflag::csn-5; gfp::fbf-1* and
191 control. Although PLA signal with FBF-1 was not statistically different from background,
192 it's possible that FBF-1 could transiently interact with CSN-5, and this assay might not
193 effectively capture those types of interactions. Nonetheless, this data suggests that
194 FBF-2 interacts with CSN-5 *in vivo*.

195

196 **COP9 is required to maintain FBF-1/2, but not PUF-3 protein levels in stem and**
197 **progenitor cells**

198 In *C. elegans*, CSN-5 was previously identified as an interacting partner of germline
199 proteins, GLH-1 and GLH-3 (Smith et al., 2002), and found to promote accumulation of
200 GLH-1 (Orsborn et al., 2007). Therefore, we hypothesized that CSN-5 might similarly
201 promote FBF accumulation and aimed to test FBF levels in the germlines where *csn-5*
202 function was disrupted. The effect of CSN-5 on FBFs may or may not depend on the
203 COP9 complex (Tomoda et al., 1999; Wei et al., 2008; Yoshida et al., 2013). To
204 distinguish COP9-dependent and independent roles of CSN-5, we additionally
205 documented FBF levels in mutants of two COP9 subunits, *csn-2* and *csn-6*. If the whole
206 complex were required for specific functions, we would expect to see the same, or very
207 similar, phenotypes across all *csn(loss-of-function, lf)* mutants, as all mutations used in
208 this study are expected to be null alleles (Brockway et al., 2014; Fig. S6; Materials and
209 Methods). Furthermore, previous studies indicate that without CSN2 and CSN6, COP9
210 complex cannot readily incorporate CSN5, and thus remains inactive (Lykke-Anderson
211 et al., 2003; Birol et al., 2014; Lingaraju et al., 2014). Additionally, it is unlikely that adult
212 *csn(lf)* germlines would have residual CSN protein from maternal contribution (Oron et
213 al., 2002). We quantified the total FBF protein levels in adult *csn(lf)* mutant worms by
214 Western blotting with antibodies to the endogenous FBF-1 or epitope-tagged
215 endogenous 3xV5::FBF-2 (Shin et al., 2017), and used tubulin as a loading control. We
216 found the most drastic reduction of FBF-1 protein level in *csn-5(lf)* (0.24-fold of the wild-
217 type levels; $p<0.005$; Fig. 4A, B), whereas *csn-6(lf)* and *csn-2(lf)* were affected weaker
218 (0.39-fold and 0.68-fold; $p<0.01$; $p<0.05$, respectively; Fig. 4A, B). Furthermore, FBF-1
219 protein levels in the *csn-5(lf)* mutant were significantly lower than those in the *csn-2(lf)*
220 mutant ($p<0.05$; Fig. 4B). Immunostaining of the *csn-5(lf) and csn-6(lf)* mutants
221 confirmed the loss of signal in the distal SPCs (Fig. 4D-G), where FBFs are normally
222 expressed, and suggested that the reduction of FBF-1 protein does not simply result
223 from a decrease in stem cell numbers. The stronger FBF-1 protein reduction in *csn-5(lf)*
224 implies that CSN-5 might be promoting the accumulation of FBF-1 independently of the

225 COP9 complex, since the relative amounts of FBF-1 would be similar across all mutants
226 otherwise. Surprisingly and distinctly, we observed a significant reduction of 3xV5::FBF-
227 2 in all *csn(lf)* mutants by Western blot (0.29-fold; $p<0.0001$; Fig. 4A, C) and confirmed
228 this observation by immunostaining (Fig. 4H-K), suggesting COP9-dependence. We
229 conclude that CSN-5, as well as COP9, promote FBF steady-state accumulation.

230 The reduction in FBF-1/2 protein levels may be caused by a decrease in *fbf* transcripts
231 or by an effect on FBF proteins. To start distinguishing these possibilities, we tested if
232 *csn(lf)* affects the steady-state levels of *fbf-1/-2* mRNAs using quantitative PCR. Using
233 *unc-54* (myosin heavy chain) as a control and normalizing mRNA abundance to a
234 reference gene, *act-1* (actin), we observed a reduction in *fbf-1* mRNA abundance in
235 each of the mutants but due to high variability the difference was not statistically
236 significant (Fig. S2). However, we observed a statistically significant reduction of *fbf-2*
237 mRNA abundance in each *csn(lf)* mutant compared to wild type ($p<0.0001$; Fig. S2). By
238 contrast, we did not observe a decrease in *unc-54* mRNA in any *csn(lf)* mutant (Fig.
239 S2). As the effects of all *csn(lf)* mutants on the levels of *fbf* transcripts were similar, we
240 conclude that COP9 signalosome is required for normal steady state levels of *fbf*
241 mRNAs. However, distinct levels of FBF-1 protein in *csn-2(lf)* vs. *csn-5(lf)* mutant
242 backgrounds (Fig. 4A, B) suggest that CSN-5 might additionally promote FBF-1 protein
243 accumulation.

244 In addition to FBF-1 and FBF-2, *C. elegans* germline stem and progenitor cells express
245 three other members of PUF-family RNA-binding proteins, PUF-3, PUF-11, and PUF-8
246 (Haupt et al., 2020; Ariz et al., 2009; Racher and Hansen, 2012). Although we were
247 unable to determine if CSN-5 interacts with other PUF proteins *in vitro*, we aimed to test
248 whether the levels of another PUF were affected by *csn-5(lf)*. We investigated PUF-3,
249 for which a tagged *3xv5* allele is available (Haupt et al., 2020). PUF-3 is expressed at
250 low levels in the progenitor zone and reaches its strongest expression in the oocytes
251 (Haupt et al., 2020; Spike et al., 2022). For direct comparison with FBFs, we focused on
252 the progenitor zone and immunostained *csn-5(lf) v5::puf-3* germlines with antibodies to
253 V5-tag (Fig. 4L, M). We observed a significant increase in SPC 3xV5::PUF-3 levels (1.3-
254 fold; $p<0.0001$; Fig. 4N) in the *csn-5(lf)* background, opposite of what we observe with

255 FBF levels (Fig. 4B, C). We conclude CSN-5 contribution to protein accumulation is
256 specific for FBFs in contrast to other PUF-family members, such as PUF-3.

257

258 **COP9 subunit mutants have reduced numbers of stem cells that continue to**
259 **proliferate and enter meiosis**

260 If CSN-5 facilitates FBF function in the germline, we expect *csn-5(lf)* mutation to cause
261 developmental defects similar to those caused by *fbf-1/2(lf)*. Because FBFs regulate the
262 switch from mitosis to meiosis in the *C. elegans* germline (Crittenden et al., 2002;
263 Wickens et al., 2002) and therefore affect the size of its stem and progenitor cell (SPC)
264 population, we quantified the number of SPCs in *csn(lf*) mutants. We dissected and
265 stained adult germlines with the antibodies specific to proliferating cells in the progenitor
266 zone, anti-REC-8, to visualize the SPC zone (Fig. 5Ai-iv; Hansen et al., 2004). We
267 observed that all *csn(lf)* mutants had reduced numbers of SPCs compared to the wild
268 type (p<0.0001, Fig. 5B), which is in general agreement with a previous report
269 (Brockway et al., 2014). The *csn-6(lf)* and *csn-5(lf)* mutants had the most drastic
270 reduction in SPCs, whereas the *csn-2(lf)* SPCs were less affected (p<0.01, Fig. 5B).
271 Although a decrease in SPCs is not a phenotype unique to *fbf(lf)*, it is consistent with
272 compromised FBF function. To test whether *csn-5* functions in the same genetic
273 pathway as *fbfs*, we quantified the number of SPCs in *csn-5(lf)* following *fbf* knockdown
274 with RNAi that targets both *fbf-1* and *fbf-2* (we were not able to generate a triple-mutant
275 strain because of incompatibility between *mIn1* and *nT1* balancers). When cultured at
276 higher temperatures (24°C), *fbf(RNAi)*-treated animals maintain reduced numbers of
277 SPCs (Merritt and Seydoux 2010; Hansen and Schedl 2013). Efficacy of RNAi
278 treatment was confirmed by germline masculinization of *csn-5(lf)/nT1* as seen in *fbf-1/-*
279 *2(lf)* mutants (Crittenden et al., 2002). We observed no additive effect on SPC number
280 in *csn-5(lf) fbf(RNAi)* background (Fig. S3A), supporting the hypothesis that *csn-5*
281 functions in the same genetic pathway as *fbf-1* and *fbf-2* in germline SPCs.

282 Because *csn-5(lf)* and *csn-6(lf)* mutant germlines are visibly smaller than wild type (Fig.
283 5Aiii-iv, and full germline images in Fig. 6Aiii-iv), we tested whether their germline SPCs
284 arrested cell cycle progression. To test whether germline SPCs continue to proliferate

285 and enter meiosis, we performed EdU incorporation assays combined with
286 immunostaining with antibodies specific for mitotic M-phase or proliferating cells in the
287 progenitor zone. First, young adult germlines were labeled with the thymidine analog 5-
288 ethinyl-2'-deoxyuridine (EdU) for 4 hours and stained for phospho-histone H3 (pH3) to
289 identify cells in S-phase and M-phase respectively, and scored by how many germlines
290 were positive for: pH3, EdU incorporation, both pH3 and EdU incorporation, or had
291 neither (Fig. 5C, D). We found that approximately 90% of *csn-5/-6(lf)* germlines had
292 SPCs positive for EdU incorporation and/or pH3, together, indicating active cell cycle
293 progression. Next, we tested if *csn-5/-6(lf)* SPCs were capable of meiotic entry by
294 staining adult gonads that have been labeled with EdU for 14 hours with REC-8, and
295 scoring how many germlines had EdU-positive cells that were able to initiate meiosis
296 and move beyond the SPC zone as detected by the loss of REC-8 staining (Fox et al.,
297 2011; Kocsisova et al., 2018). Approximately 98% and 95% of *csn-5/-6(lf)* germlines,
298 respectively, exhibited progression of EdU-positive cells into meiosis (Fig. 5E-G).
299 Additionally, we observed weaker EdU signal in the two *csn(lf)* mutants and found that
300 EdU-positive cells accumulated slower than in the wild type despite identical EdU
301 treatment conditions (data not shown, see Materials and Methods for detail). We
302 conclude that *csn-5(lf)* and *csn-6(lf)* germline SPCs sustain proliferation and meiotic
303 entry, although both cell cycle and meiotic entry appear slower than in the wild type.

304

305 **Defective oogenesis in COP9 subunit mutants**

306 FBFs play a role in germline sex determination by regulating the spermatogenesis to
307 oogenesis switch (Zhang et al., 1997; Crittenden et al., 2002), so we assessed if
308 germline sex determination was affected in the *csn(lf)* mutants. The majority of *csn-6(lf)*
309 and *csn-5(lf)* mutants failed to produce oocytes and generated only sperm (Fig. 6Aiii-iv,
310 B). This raised the possibility that downregulation of FBF protein in these *csn(lf)* genetic
311 backgrounds might be secondary to germline masculinization, as previously observed
312 for GLD-1 (Jones et al., 1996). To address this, we compared FBF levels in the male
313 versus hermaphrodites of the same genetic background and observed no significant
314 difference in FBFs (Fig. S4A), suggesting that the decrease in FBF protein levels is

315 likely a direct consequence of the *csn-5(lf)* and *csn-6(lf)*. Although germline
316 masculinization can result from a variety of genetic causes (reviewed in Ellis, 2021), it is
317 consistent with a decrease in *fbf* function (Zhang et al., 1997; Crittenden et al., 2002).
318 Curiously, the *csn-2(lf)* mutant had a clearly distinct phenotype where most germlines
319 could still form oocytes (Fig. 6Aii, B). As we observed significantly more FBF-1 protein
320 in *csn-2(lf)* than in *csn-5(lf)* (Fig. 4B), we next combined *csn-2(lf)* with *fbf-1(lf)* to test if
321 the switch to a female germ cell fate in *csn-2(lf)* was dependent on FBF-1. We found the
322 levels of masculinization in *csn-2(lf); fbf-1(lf)* germlines increased to 82%, similar to
323 those observed in *csn-5(lf)* (83%; Fig. 6B). This is consistent with the interpretation that
324 the reduction of FBFs underlies disrupted sperm/oocyte switch in *csn-5/-6(lf*) mutants.

325 To investigate molecular markers of oogenesis in *csn-5(lf)* germlines, we examined
326 expression of PUF-3 that is highly expressed in proximal pachytene at the start of
327 oogenesis and throughout oocytes (Haupt et al., 2020; Spike et al., 2022; Fig. 6Di). We
328 observed the absence of 3xV5::PUF-3 at the proximal end of *csn-5(lf)* germlines in the
329 presence of sperm, suggesting a failure of the switch to oogenesis (Fig. 6Dii, Eii). This
330 supports our initial interpretation that *csn-5(lf)* mutant germlines fail to promote female
331 fate, rather than arrest oogenic pachytene cells at the transition to diplotene.

332

333 **CSN-5's role in germline sex determination is largely independent of COP9 and**
334 **cell autonomous**

335 We hypothesized that the similar germline stem cell and sex determination phenotypes
336 observed in *csn-5(lf)* and *csn-6(lf)* mutants were caused by a decrease in the levels of
337 CSN-5 protein in *csn-6(lf)*. Indeed, we observed that the levels of 3xFLAG::CSN-5
338 transgene in a *csn-6(lf)* background decrease by approximately 60% compared to the
339 control (Fig. S4B), similar to a previous observation of a decrease in endogenous CSN-
340 5 levels after a knockdown of *csn-6* (Miller et al., 2009). We aimed to test whether CSN-
341 5-dependent, COP9-independent phenotypes might be rescued by increasing *csn-5*
342 copy number in the *csn-6(lf)* background. To this end, we first tested whether the
343 *3xflag::csn-5* transgene was able to complement the *csn-5(lf)* mutant and observed
344 complete rescue of fertility (Table 1). Next, we introduced the *3xflag::csn-5* transgene

345 into *csn-6(lf)* and found that an extra copy of *csn-5* was able to partially rescue germline
346 masculinization of *csn-6(lf)*, resulting in phenotypes similar to those of *csn-2(lf)* (Fig.
347 6C). However, it was unable to rescue the low numbers of stem cells in *csn-6(lf)* (data
348 not shown). Ectopic CSN-5 in *csn-6(lf)* would be unable to rescue COP9 function
349 because in the absence of CSN-6, CSN-5 fails to incorporate into the COP9
350 holoenzyme and the complex remains enzymatically inactive (Birol et al., 2014;
351 Lingaraju et al., 2014). We conclude that the role of CSN-5 in FBF-mediated sex
352 determination does not require COP9 signalosome.

353

Table 1: Germline-expressed CSN-5 rescues fertility defect of *csn-5(lf)*

Genotype	% Fertile	*n*
3xv5::fbf-2(q932); csn-5(ok1064)	0	>500
csn-5p::3xflag::csn-5; csn-5(ok1064)	100	>500
gld-1p::3xflag::csn-5; csn-5(ok1064)	100	311
gld-1p::3xflag::csn-5(D152N); csn-5(ok1064)	46.4*	110

n indicates number of germlines scored.
* Fertile animals were able to produce embryos that failed to hatch

354

355 Because CSN-5 is expressed in both germline and somatic tissues (Smith et al., 2002;
356 Miller et al., 2009), we aimed to test whether its function was required in the soma or the
357 germline. We generated a *3xflag::csn-5* transgene using the *gld-1* promoter, which is
358 expected to restrict expression to the germline (Ellenbecker et al., 2019; see Materials
359 and Methods for details), and still observed 100% rescue of fertility when incorporated
360 into the *csn-5(lf)* mutant background (Table 1). This suggests that the effects of *csn-5*
361 on sex determination are likely cell-autonomous within the germline. We next tested
362 whether the *csn-5* function in promoting female germ cell fate was dependent on its
363 deneddylating activity by generating a catalytically inactive CSN-5(D152N) transgene,
364 based on a previously reported catalytic mutant (Cope et al., 2002; Peth et al., 2007).
365 CSN-5(D152N) is incorporated into COP9, but fails to promote de-neddylation (Cope et
366 al., 2002); therefore, it would only rescue COP9-independent function of *csn-5*. We find
367 that 3xFLAG::CSN-5(D152N) transgene can partially rescue oogenesis in *csn-5(lf)*
368 (Table 1), suggesting that the effect of *csn-5* on germline sex determination is not

369 entirely dependent on its proteolytic activity. However, since CSN-5-mediated
370 deneddylation by COP9 is required for embryonic cell division (Pintard et al., 2003), all
371 embryos produced by the *3xflag::csn-5(D152N); csn-5(lf)* were dead. Additionally,
372 inactive CSN-5(D152N) maintains its ability to bind FBF-2 *in vitro* via GST pulldown (Fig.
373 S4C) as expected if its effect depended on interaction with FBF-2.

374

375 **CSN5 maintains FBF protein levels through multiple mechanisms**

376 To begin investigating a mechanism behind the compromised FBF accumulation and
377 function in *csn-5(lf)* mutants, we tested whether CSN-5 stabilizes FBF proteins by
378 interfering with their proteasome-mediated degradation. If true, we expect that
379 disruption of the proteasome function in *csn-5(lf)* mutants would restore FBF protein
380 levels. To test this hypothesis, we knocked down *pbs-6*, a catalytic subunit of the 20S
381 proteasome, in the *rrf-1(lf)* genetic background to preferentially direct the RNAi
382 knockdown to the germline (Sijen et al., 2001; Kumsta and Hansen, 2012). We
383 observed a complete rescue of both steady-state FBF-1 ($p<0.01$) and 3xV5::FBF-2
384 ($p<0.05$) protein levels in *rrf-1(lf); csn-5(lf)* following *pbs-6(RNAi)* (Fig. 7A-D). We were
385 unable to assess the effects of this rescue on SPC zone size as *pbs-6(RNAi)* on the
386 control strain *rrf-1(lf); 3xv5::fbf-2(q932)* reduced the number of SPCs similar to *csn-5(lf)*
387 (data not shown). Unexpectedly, crossing *csn-5(lf)* into *rrf-1(pk1417)* genetic
388 background largely suppressed the failure of oogenesis and allowed formation of
389 abnormal oocytes in 79% of examined germlines precluding testing whether *pbs-*
390 *6(RNAi)* rescued oogenesis (Fig. S5). Understanding the nature of this suppression,
391 including whether it results from the loss of *rrf-1* or a different background or linked
392 mutation, remains the subject of future research. Since we previously observed a
393 decrease in *fbf-1/2* transcript levels in *csn-5(lf)* background (Fig. S2), we next
394 determined whether the rescue of FBF protein accumulation upon proteasome
395 disruption was mediated by an increase in *fbf* mRNA abundance. Quantification of
396 steady-state *fbf* mRNA levels by qRT-PCR revealed that *pbs-6(RNAi)* did not increase
397 *fbf* transcript levels (Fig. 7E). We conclude that CSN-5 promotes the stability of FBF
398 proteins.

399 The main enzymatic activity of the COP9 signalosome is deneddylation of cullin
400 subunits of **S**kp1-**c**ullin 1-**F**-box (SCF) ubiquitin ligases to promote turnover of the SCF
401 targets (Lyapina et al., 2001; Cope et al., 2002; Pintard et al., 2003). Therefore, some
402 phenotypes of *csn(lf)* mutants could result from the increased neddylation. Notably, a
403 knockdown of *C. elegans* NEDD8 homolog, *ned-8*, has been shown to partially
404 suppress meiotic defects seen in *csn(lf)* mutants (Brockway et al., 2014). By contrast,
405 the effects of mammalian CSN5 on stability and function of its protein partners HIF-1a
406 and E2F1 are independent of its deneddylase activity (Bemis et al., 2004; Hallstrom and
407 Nevins, 2006). To investigate whether *csn-5* is affecting FBFs stability via
408 deneddylation, we performed *ned-8(RNAi)* on the *csn-5(lf)* mutant (we were unable to
409 generate a *ned-8; csn-5* mutant strain for analysis due to larval arrest observed in the
410 homozygous *ned-8* mutant, Brockway et al., 2014; data not shown). We quantified
411 expression of FBF-1 and V5::FBF-2 in distal mitotic cells simultaneously by co-staining
412 the treated germlines with respective antibodies. Interestingly, we observed a partial
413 rescue of FBF-2, but not FBF-1, levels in *ned-8(RNAi)*-treated *csn-5(lf)* mutants
414 (increased to 0.76-fold on average; Fig. 8A-F). We conclude that CSN-5 contributes to
415 FBF-1 and FBF-2 maintenance through two mechanisms, stabilizing FBF-1 independent
416 of the deneddylating activity, and promoting FBF-2 accumulation through a combination
417 of deneddylation-dependent and -independent mechanisms. Consistent with the partial
418 rescue of FBF-2 function, we find that *ned-8(RNAi)* treatment of *csn-5(lf)* partially
419 rescues SPCs numbers (Fig. 8G). Additionally, we observed that *ned-8(RNAi)*
420 completely rescues oogenesis (Fig 8H). However, interpretation of this result is
421 complicated by the fact that neddylation is essential for the function of cullin-based E3
422 ubiquitin ligases (Duda et al., 2008; Saha and Deshaies, 2008; Boh et al., 2011), and a
423 cullin-based CUL-2/FEM-1/FEM-2/FEM-3 ubiquitin ligase is required for
424 spermatogenesis (Starostina et al., 2007). Therefore, it is unclear whether the rescue of
425 oogenesis is solely due to an increase in FBF-2 or also to downregulation of CUL-
426 2/FEM-1/FEM-2/FEM-3 activity.

427

428 **Discussion:**

429 In this study, we have identified the COP9 signalosome component CSN-5 as a new
430 interacting partner of PUF-family RNA-binding proteins FBF-1 and -2, and documented
431 both COP9-independent and -dependent CSN-5 functions in promoting stem and
432 progenitor cell (SPC) proliferation as well as female fate in *C. elegans* germline.
433 Analysis of *csn-5(lf)* mutant background uncovered instability of FBF-1 and -2 proteins
434 that is counteracted by CSN-5. We propose that CSN-5 maintains steady-state levels of
435 FBF-1 and FBF-2 in the *C. elegans* germline by distinct mechanisms (Fig. 9).

436

437 ***An interaction between MPN and PUF domains***

438 We found the interaction between CSN-5 and FBFs in a yeast two-hybrid screen and
439 confirmed it with GST pulldowns of recombinant proteins (Fig. 1B, D). Curiously, CSN-5
440 hasn't been reported in the prior published yeast two hybrid screen using FBF-1 as a
441 bait (Kraemer et al., 1999; Eckmann et al., 2002), but it might be a result of differences
442 in prey library construction. We found that the direct interaction between PUF-family
443 proteins (FBF-1, -2, and PUM1) and CSN5 homologs is mediated by conserved
444 structured domains, the RBD and the MPN domain respectively (Fig. 2A, C, F).
445 However, not all PUF RBDs bind CSN5 and not every type of MPN domain binds PUF
446 proteins. At this time, the determinants of PUF/MPN binding are enigmatic. As reviewed
447 in Wickens et al., 2002, PUF domains of PUM1 and PUM2 are very similar to each
448 other (over 90% identical; Spassov and Jurecic, 2002), yet they exhibit distinct
449 interaction properties with the $CSN5^{MPN}$ (Fig. 2F). On the other hand, FBF-1 and FBF-2
450 belong to a separate, nematode-specific clade of PUF RBDs, with less than 30%
451 identity to PUM RBDs (Wickens et al., 2002; Spassov and Jurecic, 2003), yet both are
452 able to interact with $CSN\text{-}5^{MPN}$. This raises the question whether additional PUF
453 proteins out of ten described in *C. elegans* also bind to CSN-5. In addition to FBFs,
454 germline stem cells express PUF-3 and PUF-11 that cluster into a nematode-specific
455 subfamily related to FBFs (Haupt et al., 2020) and PUF-8 that is closer to human and
456 *Drosophila* homologs (Ariz et al., 2009; Racher and Hansen, 2012). We were not able to

457 test association between CSN-5 and PUF domains of PUF-3, -11, and -8 due to
458 difficulties with recombinant PUF expression. If these interactions do exist, it is possible
459 that some of the effects of *csn-5(lf)* are due to downregulation of additional germline
460 PUFs. However, we do not observe a downregulation of PUF-3 in *csn-5(lf)* stem cells
461 (Fig. 4L-N), suggesting specificity towards FBFs.

462 Similar to CSN-5, CSN-6 contains an MPN domain (Birol et al., 2014). However, CSN-
463 6's MPN domain could only bind FBF-2's RBD at much higher concentrations than
464 CSN-5 (Fig. 2E). Taken together, this suggests a selective association between a
465 subset of PUF RNA-binding proteins and their specific MPN domain-containing
466 partners. In the future, these selective interactions can help elucidate the sites
467 mediating binding between these proteins.

468 We further find *in vivo* association between CSN-5 and FBF-2 by proximity ligation
469 assay (Fig. 3). Although the *in vivo* proximity signal between CSN-5 and FBF-1 did not
470 reach statistical significance, it's possible that the interaction of CSN-5 with FBF-1 might
471 be unstable or transient, and thus remain undetectable with PLA. In line with this, co-
472 immunoprecipitation has not recovered CSN-5 as an FBF-1 interactor (Friend et al.,
473 2012). Additionally, both CSN-5 and FBF-2 are present in P granules and thus might
474 interact more frequently compared to FBF-1, which does not localize to P granules
475 (Smith et al., 2002; Voronina et al., 2012; Marnik et al., 2019). Alternatively, FBF-1
476 might be indirectly regulated by CSN-5. Nonetheless, here, we demonstrate that both
477 FBFs require CSN-5 for proper accumulation and function.

478

479 ***CSN-5 promotes FBF accumulation***

480 CSN-5 and its homologs promote stabilization of their interaction partners (Bemis et al.,
481 2004; Orsborn et al., 2007). We demonstrate that CSN-5 is similarly involved in
482 stabilizing FBFs, as both FBFs are significantly reduced in *csn(lf)* mutants (Fig. 4A-K).
483 We find that FBF-1 is most significantly reduced in *csn-5(lf)*, compared to *csn-6(lf)* or
484 *csn-2(lf)* (Fig. 4A, B), suggesting that *csn-5* employs an additional mechanism

promoting FBF-1 accumulation, independent of the COP9 complex. Conversely, we find that FBF-2 is depleted similarly in the *csn(lf)* mutants (Fig. 4A, C), suggesting the entire complex might promote FBF-2 protein accumulation. Interestingly, we also observed a reduction of *fbf* mRNAs in the *csn(lf)* mutants (Fig. S2), indicating that the entire COP9 complex is needed to maintain steady-state transcript levels. As reviewed in Chamovitz, 2009, a clear understanding of the COP9 complex in regulating transcription, outside the realm of stabilizing transcription factors and thus affecting steady-state transcript levels, remains somewhat elusive. Taken together, we conclude that there are both COP9-independent and –dependent functions of CSN-5 regulating FBF protein levels. We further demonstrate that the reduction of FBFs is likely a direct effect of *csn(lf)* and not a consequence of germline masculinization, as seen with other RNA-binding proteins such as GLD-1 (Jones et al., 1996), as FBF levels were not significantly different in males versus hermaphrodites of the same genetic background (Fig. S4Ai-iv). This function of CSN-5 in FBF protein accumulation, regardless of COP9-dependence, reveals a previously unappreciated role for CSN-5 and also provides the first insight regarding the post-translational regulation of PUF family members FBF-1 and -2. By contrast, we find that CSN-5 does not promote germline stem cell PUF-3 protein accumulation, as seen with FBFs, but might have the opposite effect as we observed a significant increase of PUF-3 accumulation in SPCs of the *csn-5(lf)* mutant germlines (Fig. 4L-N). Recent findings suggest that accumulation of PUF-3 and PUF-11 in the distal mitotic cells is restricted by a TRIM-NHL protein NHL-2 (Brenner et al., 2022) and their degradation at the oocyte to embryo transition is mediated by ubiquitin proteasome system (Spike et al., 2022). It is unclear whether CSN-5 impacts PUF-3 accumulation directly or indirectly and how that might compare to other mechanisms regulating PUF-3 expression. However, the effect on PUF-3 accumulation is distinct from that seen with FBFs indicating CSN-5 specifically regulates FBFs and phenotypes observed in *csn-5(lf)* are not due to a downregulation of multiple PUF proteins.

513 ***CSN-5 promotes FBF protein stability***

514 In this work, we uncovered intrinsic instability of FBF proteins in *csn-5(lf)* mutant
515 background suggesting that *csn-5* promotes FBF accumulation through protecting them
516 from degradation. FBF protein levels in the *csn-5(lf)* genetic background were rescued
517 by disrupting proteasome-mediated degradation without affecting *fbf* transcript levels
518 (Fig. 7). Interestingly, we find that FBF-2, but not FBF-1, levels are partially rescued in
519 the *csn-5(lf)* genetic background with *ned-8(RNAi)* (Fig. 8A-F). This suggests that CSN-
520 5 likely regulates FBF-1 in a COP9-independent manner, whereas regulation of FBF-2
521 might involve a combination of COP9-dependent and –independent mechanisms.
522 These distinct mechanisms of FBF-1/-2 regulation by CSN-5 are also supported by the
523 observation that FBF-1 levels were most drastically reduced in *csn-5(lf)* whereas FBF-2
524 levels were equally reduced among all mutants (Fig. 4). As cullins are the only known
525 targets of COP9-mediated deneddylation (Qin et al., 2020), it's not surprising we have
526 never detected an accumulation of neddylated FBF-2 by Western blot analysis of *csn(lf)*
527 mutant lysates. Although stabilization of FBF-2 requires CSN-5 in the context of COP9,
528 the mechanistic connection between COP9-mediated cullin deneddylation and
529 accumulation of (non-cullin) FBF-2 awaits further study.

530

531 **CSN-*5 contribution to germline sex determination***

532 In this study, we found that *csn-5* contributes to the regulation of germline sex
533 determination through maintenance of FBF protein levels. Loss of function of both *csn-5*
534 and *csn-6* led to a failure to generate oocytes in the majority of mutant germlines (Fig.
535 6A, B). This loss of oogenic fate was confirmed through a lack of detectable expression
536 of 3xV5::PUF-3 in the proximal pachytene cells of *csn-5(lf)* (Fig. 6D). By contrast,
537 oocytes formed in the majority of *csn-2(lf)* mutant germlines (Fig. 6Aii, B), and this
538 residual oogenesis in *csn-2(lf)* was dependent on FBF-1 as levels of germline
539 masculinization in *csn-2(lf); fbf-1(lf)* increased to those seen in *csn-5(lf)* (Fig. 6B). The
540 function of *csn-5* in germline sex determination appears to be cell-autonomous as the
541 *3xflag::csn-5* transgene driven by the *gld-1* promoter (Ellenbecker et al., 2019) and

542 expected to only be expressed in the germline rescued oocyte formation to 100%,
543 similar to the *3xflag::csn-5* transgene under the control of *csn-5* promoter (Table 1).

544 Does the mutation of *csn-5* compromise other subunits of the COP9 complex?
545 Previously-published work in human cells, *Drosophila* larvae, and with recombinant
546 proteins suggests that the loss of CSN5 leaves the remainder of COP9 subunits largely
547 intact and assembled, except unable to carry out deneddylation of cullin substrates
548 (Oron et al., 2002; Groisman et al., 2003; Yun et al., 2004; Peth et al., 2007; Sharon et
549 al., 2009). Therefore, we interpret *csn-5(lf)* phenotypes as reflecting the loss of CSN-5
550 protein and deneddylation, but not affecting the other COP9 subunits. By contrast, loss
551 of several other COP9 subunits results in downregulation of CSN5, as observed for
552 knockdowns of human CSN1 and CSN3 (Peth et al., 2007) as well as for knockdown or
553 mutation of *C. elegans csn-6* (Miller et al., 2009; Fig. S4B). Therefore, care must be
554 taken to distinguish whether any phenotypes of *csn-6(lf)* result from the secondary loss
555 of CSN-5. We approached this by introducing an additional copy of *csn-5* into *csn-6(lf)*
556 genetic background, which was sufficient to rescue oogenesis (Fig. 6C). This suggests
557 that defective oogenesis in *csn-6(lf)* results from the secondary loss of CSN-5.
558 Additionally, this result argued that CSN-5 is sufficient to promote oogenesis in the
559 absence of CSN-5/CSN-6 heterodimer, since *csn-6(lf)* is a null allele where maternal
560 protein stockpile is expected to be depleted (Brockway et al., 2014). Overall, we
561 conclude that CSN-5 is able to promote oogenesis outside of COP9 holoenzyme.

562 Finally, several lines of evidence suggest that CSN-5 can promote female germ cell fate
563 independent of deneddylating activity. First, *csn-2(lf)* is expected to disrupt COP9-
564 dependent deneddylation, yet it still allows oogenesis in ~70% of mutant germlines.
565 Second, CSN6 is critically required for COP9-dependent deneddylation (Birol et al.,
566 2014), yet *3xflag::csn-5* rescues oogenesis in *csn-6(lf)* genetic background. Third, *csn-5*
567 can support considerable oogenesis independent of its deneddylating activity as we
568 observe a rescue of fertility to ~46% in the catalytically inactive, germline-specific,
569 *3xflag::csn-5(D152N); csn-5(lf)* (Table 1). An observation that appears in conflict with
570 this conclusion is the 100% rescue of oogenesis by *ned-8(RNAi)* in *csn-5(lf)* background
571 (Fig. 8H). However, *ned-8(RNAi)* did not affect FBF-1 levels and rescued FBF-2

572 amounts only in ~63% germlines (Fig. 8A, B), suggesting that the rescue of oogenesis
573 is independent of FBF levels in at least 37% of germlines. This FBF-independent
574 oogenesis might be explained by a reduction in activity of cullin-based E3 ligase CUL-
575 2/FEM-1/FEM-2/FEM-3 resulting from downregulation of neddylation via *ned-8*
576 knockdown. Neddylation is required for the function of all cullin-based E3 ligases (Duda
577 et al., 2008; Saha and Deshaies, 2008; Boh et al., 2011), and CUL-2/FEM-1/FEM-
578 2/FEM-3 is required for spermatogenesis to degrade TRA-1 (Starostina et al., 2007).
579 The CUL-2/FEM-1/FEM-2/FEM-3 complex functions downstream of FBFs in germline
580 sex determination pathway (Ellis, 2021) and *fem-3* is epistatic to *fbfs* (Zhang et al.,
581 1997). Therefore, it is possible that *ned-8(RNAi)* indirectly circumvents the requirement
582 for *csn-5* in oogenesis and that the contribution of COP9-mediated deneddylation to
583 germline sex determination is through maintaining the balance of
584 neddylated/deneddylated CUL-2/FEM-1/FEM-2/FEM-3.

585

586 ***CSN-5 role in stem cell maintenance***

587 We find that both CSN-5 and COP9 signalosome are required for germline stem cell
588 maintenance in *C. elegans*. Our findings are consistent with a previous report in
589 *Drosophila* ovarian germline stem cells (Pan et al., 2014), and identify FBFs as a
590 specific target of CSN-5 regulation relevant for stem cell maintenance. In agreement
591 with reduced FBF levels, we observed a significant loss of SPCs in *csn(lf)*, with the most
592 drastic decrease for *csn-5/-6(lf)* (Fig. 5A, B). Although this phenotype is consistent with
593 *fbf(lf)*, it is not exclusive to *fbf(lf)* and could be caused by *csn(lf)* affecting other stem cell
594 regulators. However, we found that *csn-5* functions within the same genetic pathway as
595 *fbfs* when we performed *fbf* knockdown in *csn-5(lf)* mutant and found no further
596 reduction in number of SPCs (Fig. S3A). Additionally, *csn-5(lf)* did not reduce the levels
597 of PUF-3 (Fig. 4L-N), further supporting the notion that it affects stem and progenitor
598 cells though regulation of FBF levels. It is still unclear whether CSN-5's function in stem
599 cell maintenance depends on the presence of other COP9 subunits as we were unable
600 to rescue SPC numbers in *csn-6(lf)* mutant by providing an extra copy of *3xflag::csn-5*.

601 This result might be due to the insufficient levels of the transgenic protein (Fig. S4B).
602 Alternatively, it remains possible that CSN-5 needs to form a heterodimer with CSN-6 to
603 promote stem cell proliferation. We couldn't establish whether stabilization of FBFs by
604 inhibiting proteasome-dependent degradation would suppress the SPC reduction in *csn-*
605 *5(lf)* since *pbs-6(RNAi)* caused reduction of SPC numbers in the control background
606 (data not shown) likely due to its effects on the cell cycle. However, we find a partial
607 rescue of SPC numbers in *csn-5(lf) ned-8(RNAi),* which is consistent with a partial
608 rescue of FBF-2 function, along with a partial rescue of FBF-2 protein levels (Fig. 8B,
609 G). Therefore, we conclude that deneddylation activity of CSN-5 contributes to stem cell
610 proliferation, possibly through regulation of FBF-2 levels. We considered whether *csn-*
611 *5(lf) ned-8(RNAi)* produced a germline state reminiscent of *fbf-1(lf)* since we observed
612 an increase in FBF-2 protein without a rescue of FBF-1. *fbf-1(lf)* mutation results in a
613 smaller progenitor zone compared to the wild type germlines (Lamont et al., 2004).
614 However, the number of SPCs in *csn-5(lf) ned-8(RNAi)* (~0.62x of the wild type on
615 average, Fig. 8G) is smaller than that of *fbf-1(lf)* mutant (~0.85x of the wild type; Wang
616 et al., 2020), suggesting that the partial rescue of FBF-2 levels is not sufficient to
617 recapitulate its full functionality.

618 A number of previously characterized mutants of splicing factors exhibit a combination
619 of defective female fate specification as well as underproliferated germlines, reminiscent
620 of those observed in *csn-5* and *csn-6* mutants (Puoti and Kimble, 1999, 2000; Belfiore
621 et al., 2004; Konishi et al., 2008; Mantina et al., 2009; Zanetti et al., 2011; Wang et al.,
622 2012). This raised the question of whether underproliferation observed in *csn-5* and -
623 *6(lf)* was linked to the failure of sperm/oocyte switch. However, we could not rescue
624 number of SPCs (data not shown) with *3xflag::csn-5; csn-6(ok1604)* despite being able
625 to rescue oogenesis (Fig. 6C), suggesting that the reduction in SPCs in *csn-6(lf)* does
626 not result from a defective switch to oogenesis. Additionally, male germlines maintain
627 similar SPC population to the hermaphrodite germlines, suggesting no intrinsic sex-
628 specific differences in stem cell numbers (Morgan et al., 2010).

629 The SPCs of *csn-5/-6(lf)* germlines continue to proliferate and enter meiosis (Fig. 5C-G)
630 indicating that the smaller germlines of these genetic backgrounds (Fig. 5A, 6A) are not

631 the result of arrested cell divisions. However, we also observed that *csn-5/-6(lf)*
632 germline SPCs incorporated EdU slower than wild type, requiring longer EdU exposures
633 to label nuclei (data not shown), suggesting a slower cell cycle. Notably, homologs of
634 COP9 complex subunits have previously been found regulating proteins involved in cell
635 cycle progression (Tomoda et al., 1999; Yang et al., 2002; Doronkin et al., 2003;
636 Yoshida et al., 2013), which might provide some explanation behind our observations in
637 the *csn(lf)* mutants. At this time, it remains unknown if the balance between proliferation
638 and differentiation is disrupted in these *csn(lf)* mutants, and further research would be
639 required to understand their cell cycle dynamics. In summary, we conclude that *csn-5*
640 promotes stem cell maintenance through regulation of FBF protein accumulation and
641 speculate this might be a conserved mechanism by which *csn-5* impacts stem cell
642 maintenance in other species.

643

644 ***Potential mechanisms behind CSN-5 stabilization of FBFs***

645 CSN-5/CSN5 is reported to interact with a number of proteins beyond components of
646 the signalosome (for examples see Tomoda et al., 1999; Bae et al., 2002; Smith et al.,
647 2002; Yoshida et al., 2013) and to promote accumulation of some of its interacting
648 partners (Bemis et al., 2004; Orsborn et al., 2007). Our work defines a novel class of
649 CSN-5 interactors, the PUF-family FBF proteins that are stabilized by CSN-5 and
650 reveals a new mechanism of CSN-5 contribution to stem cell maintenance. Based on
651 our detection of binding between the human homologs, we speculate that CSN5 might
652 similarly stabilize PUM1. The mechanism of CSN-5-dependent stabilization of its
653 partner proteins remains unclear, especially considering there might be several
654 mechanisms at play as revealed by this work. One possible mechanism suggested by
655 previous reports in both fission yeast and mammalian cells is recruitment of a
656 **de**ubiquitinating enzyme (DUB) Ubp12p/USP15 to the COP9 signalosome substrates
657 (Zhou et al., 2003; Hetfeld et al., 2005). Importantly, in several cases DUB recruitment
658 was shown to depend on CSN5 (Groisman et al., 2003; Wee et al., 2005; Liu et al.,
659 2009). Notably, if FBFs are substrates of CSN-5-associated DUBs, a transient *in vivo*

660 association between FBF-1 and CSN-5 would not be surprising. Similarly, recruitment of
661 DUBs would be consistent with the ability of catalytically-dead CSN-5(D152N) to rescue
662 FBF function. Alternatively, CSN5 was reported to directly interact with HIF1α and to
663 stabilize HIF1α in a COP9-independent manner (Bemis et al., 2004). Stabilization of
664 HIF1α was mediated by preventing proline hydroxylation of HIF1α and by interfering
665 with the association of hydroxylated HIF1α with pVHL ubiquitin ligase (Bemis et al.,
666 2004). As a third option, CSN5 metalloprotease was proposed to directly deubiquitinate
667 its binding partner (Lim et al., 2016; Liu et al., 2020). Overall, CSN-5 might be able to
668 protect FBFs from ubiquitination and thus promote their stabilization in *C. elegans*
669 germline stem cells through either of these mechanisms.

670 CSN-5 contribution to the regulation of germline stem cell proliferation through
671 stabilization of FBF proteins has major implications for understanding regulatory
672 mechanisms relevant for stem cell maintenance. Intrinsic instability of PUF-family
673 proteins counteracted by CSN-5 might reflect a general mechanism regulating the
674 abundance of essential stem cell factors and their effects on stem cell population
675 dynamics. Additionally, the function of CSN-5 in FBF stabilization may be relevant for
676 understanding cancer as CSN5 is upregulated in many human cancers (Lee et al.,
677 2011; Liu et al., 2020). Similarly, a number of cancers overexpress PUM1 and/or PUM2
678 (Guan et al., 2018; Gor et al., 2021; Shi et al., 2021; Smialek et al., 2021). This PUM
679 protein overexpression in cancer might be borne out through its stabilization via CSN5
680 and therefore reflect an unappreciated mechanism promoting cancer cell proliferation.

681 **Materials and Methods**

682 **Nematode strains and culture**

683 All *C. elegans* strains (Table S2) used in this study were cultured on New Nematode
684 Growth Medium (NNGM) plates seeded with *E. coli* OP50 as per standard protocols
685 (Brenner, 1974). c*sn(lf)* mutants used in this study were obtained from the
686 *Caenorhabditis* Genetics Center and outcrossed >8 times to wild type before analysis.
687 The strains were maintained at 20°C, unless specified otherwise.

688

689 ***csn-2(ok1288)* allele**

690 In order to determine the molecular nature of *csn-2(ok1288)* allele, we conducted PCR
691 analysis of genomic DNA as well as cDNA. Total RNA isolated from *csn-2(ok1288)*
692 hermaphrodites was reverse-transcribed using SuperScript IV reverse transcriptase
693 (Invitrogen) and amplified with the primers AGACCCAGGAAAAGTTCGGT and
694 GAGACCATCATCCAAAATTGCGT. Our analysis revealed that the 1680-nt genomic
695 deletion removes most of intron 3, exon 4, and most of intron 4. The *csn-2(ok1288)*
696 transcript is spliced from the end of exon 3 to the start of exon 5 resulting in a frameshift
697 at amino acid 238 and a premature stop codon (removing 50% of ORF; Fig. S6). The
698 full-length CSN-2 contains a PCI domain consisting of helical repeats 1-8 and a winged-
699 helix (WH) subdomain, which is followed by a C-terminal alpha helix. CSN-2 is
700 incorporated into the COP9 signalosome through association of the WH subdomain with
701 the WH subdomains of other PCI proteins and through integration of the C-terminal
702 helix into a bundle containing helices of all COP9 subunits (Lingaraju et al., 2014).
703 *ok1288* deletion removes three C-terminal PCI repeats, the WH domain, and the C-
704 terminal helix suggesting that the remaining fragment would not incorporate into COP9
705 signalosome.

706

707 **Transgenic animals**

708 All transgene constructs were generated by Gateway cloning (Thermo Fisher Scientific).
709 The two *3xflag::csn-5* transgene constructs contain either the *csn-5* promoter (1110 bp
710 upstream of the CDS) or *gld-1* promoter (1165 bp upstream of the CDS; Ellenbecker et
711 al., 2019) and both contain *csn-5* genomic coding and 3'UTR (733 bp downstream of
712 the CDS) sequences in pCFJ150 (Frokjaer-Jensen et al., 2008). The *3xflag::csn-*
713 *5(D152N)* transgene construct contains the *gld-1* promoter, *csn-5(D152N)* mutant
714 genomic coding sequence, and *csn-5* 3'UTR sequence in pCFJ150. Mutagenesis of
715 *csn-5(D152N)* was performed using a Q5 site-directed mutagenesis kit per
716 manufacturer instructions (New England BioLabs). For transgenic lines used in PLA,
717 *3xflag::csn-5* was crossed with pre-existing *patcGFP::fbf* or *patcGFP* lines (Wang et al.,
718 2020). For all *csn-5* transgenes, a single-copy insertion of the transgene was generated
719 by homologous recombination into the universal *Mos1* insertion site on LG II after Cas9-
720 induced double-stranded break (Dickinson et al., 2013; Wang et al., 2016). Transgene
721 insertion was confirmed by PCR.

722

723 **Yeast Two-Hybrid library screening and directed assays**

724 For the yeast two-hybrid screen, *fbf-2* cDNA was cloned into the pGBTK vector
725 (Clontech) and transformed into PJ68-4a yeast strain (*MAT**a** trp1-901 leu2-3,112 ura3-*
726 *52 his3-200 gal4Δ gal80Δ LYS2::GAL1-HIS3 GAL2-ADE2 met2::GAL7-lacZ*; James et
727 al., 1996). The yeast two-hybrid library was generated from the poly(A)+ mRNA isolated
728 from mixed-stage N2 nematodes using the Matchmaker kit (Clontech) as per the
729 manufacturer's protocol and transformed into Y1HGold strain (*MAT**α**, ura3-52, his3-200,*
730 *ade2-101, trp1-901, leu2-3, 112, gal4Δ, gal80Δ, met–, MEL1*). The bait and prey library
731 strains were mated and cultured on selective plates SD/-Trp, Leu, His, Ade with 1 mM
732 3-AT; the total number of screened diploids was estimated at 2.32×10^8. Out of 271
733 positive colonies, 99 (37%) were identified as *csn-5* fragments by PCR and sequencing
734 of prey plasmid inserts. For directed interaction assays, FBF-1 or FBF-2 in a bait vector
735 pGBKT7 and CSN-5 in a prey vector pGADT7 were cotransformed in PJ69-4a. Empty
736 prey vector was used as the control. Expression of c-myc tagged FBF-1 or FBF-2 and

737 HA tagged CSN-5 proteins in yeast colonies were confirmed by Western blot, see Table
738 S3 for antibody information. Serially diluted yeast cultures (at OD600 0.2) expressing *fbf*
739 bait and *csn-5* prey (or empty prey) were spotted on control or the interaction selection
740 plate SD/-Trp, -Leu, -His, -Ade (with 1mM 3-AT to inhibit leaky expression of Histidine
741 reporter) and incubated at 30°C for 4 days.

742

743 **GST pulldown assay**

744 Expression constructs containing His_6::FBF-1 and His_6::FBF-2 have been described
745 before (Wang et al., 2016). Truncated FBF expression constructs were generated by
746 PCR from full-length FBF-1 or FBF-2 and inserted into pETDuet-1 plasmid (EMD
747 Millipore). Full-length *C. elegans* CSN-5 (amino acids 1-368) and CSN-6^{MPN} (amino
748 acids 1-197) were amplified from N2 Bristol cDNA and cloned into pGEX-KG plasmid.
749 Mutant CSN-5(D152N) was generated from full-length CSN-5 using a Q5 site-directed
750 mutagenesis kit per manufacturer's instructions (New England BioLabs). Truncated
751 CSN-5 constructs were made by PCR from full-length CSN-5 and inserted into pGEX-
752 KG plasmids. Human $CSN5^{MPN}$ (amino acids 1-257) was amplified from HEK293 cDNA
753 and cloned into pGEX-KG plasmid. Human $PUM1^{RBD}$ (isoform 1, amino acids 828-1176)
754 and $PUM2^{RBD}$ (isoform 3, amino acids 706-1055) were amplified from HEK293 cDNA
755 and cloned into pETDuet-1 plasmid. All constructs were sequenced and transformed
756 into *Escherichia coli* strain BL21(DE3) for expression. Expression of His-tagged FBF
757 protein constructs was induced with 0.1 mM IPTG at 15°C for 20-24 hours. Expression
758 of GST alone or GST-tagged CSN protein constructs was induced with 0.1 mM
759 isopropyl β-D-1-thiogalactopyranoside (IPTG) at 37°C for 4.5 hours. Pellets of induced
760 bacteria were collected and resuspended in lysis buffer (20 mM Tris pH 7.5, 250 mM
761 NaCl, 10% glycerol, 1 mM $MgCl_2$, 0.1% Triton X-100) containing 10 mM beta-
762 mercaptoethanol (BME), 1 mM phenylmethylsulfonyl fluoride (PMSF), 1x Roche
763 protease inhibitor cocktail, 0.5 mg/ml lysozyme, and 6 µg/ml DNase I, rotated at 4°C for
764 1 hour to lyse, and cleared by centrifugation at 1110 *g* for 20 min. Cell lysates of GST
765 alone or GST-tagged CSN constructs were bound to glutathione beads in 20 mM Tris
766 pH 7.5, 250 mM NaCl, 10% glycerol, 0.1% Triton X-100, 10 mM BME, 1 mM PMSF, and

767 1x Roche protease inhibitor cocktail for 1 hour at 15°C. Binding reactions with His_6-
768 tagged preys were incubated at 15°C for 3 hours and washed four times with 10 mM
769 Tris pH 7.5, 150 mM NaCl, 0.1% NP-40, and 0.5 mg/ml BSA. For elution, beads were
770 heated to 95°C for 5 minutes in sodium dodecyl sulfate (SDS) sample buffer and 10 mM
771 dithiothreitol (DTT). To test if the FBF-2/CSN-5/-6 binding interaction is RNA-dependent,
772 50 µg/ml RNase A was added to His_6::FBF-2 lysate before incubation with GST alone or
773 GST::CSN-5/-6.

774

775 **Western blot analysis**

776 Protein samples from pulldown assays were separated using Mini-PROTEAN TGX 4-
777 20% precast gels (Bio-Rad,) and visualized using either Coomassie, stain-free
778 chemistry, or by Western blotting. For anti-His probing, all eluates were treated the
779 same. For anti-GST probing, GST negative control eluate was diluted 8-fold further than
780 GST::CSN constructs to avoid overexposure. See Table S3 for antibody information.
781 Expression, and attachment to GSH beads, of all GST alone and GST-tagged
782 constructs was confirmed for each pulldown experiment.

783 To analyze FBF protein levels in *csn(lf)* mutants, 50-100 young adult worms of each
784 genotype were picked from synchronous cultures, and lysed in SDS-PAGE sample
785 buffer containing 2.8% SDS and 75mM DTT by boiling for 15 minutes prior to SDS-
786 PAGE gel electrophoresis. Protein samples were separated on a 7.5% or 4-20% gel
787 (Bio-Rad) and transferred to a 0.2 µm PVDF membrane (EMD Millipore). After transfer,
788 membranes were blocked in 50 mM Tris pH 7.5, 180 mM NaCl, 0.05% Tween 20 with
789 5% non-fat dry milk powder, and probed with antibodies (see Table S3) diluted in
790 blocking solution. Membranes were developed using Luminata Crescendo Western
791 HRP substrate (EMD Millipore) and visualized using Bio-Rad ChemiDoc™ MP Imaging
792 System. Band intensities were quantified using Image Lab software version 5.1.

793

794 **Proximity ligation assay (PLA)**

795 Duolink® PLA was performed on dissected *C. elegans* gonads following a modified PLA
796 protocol as described (Day et al., 2020; Wang et al., 2020). Fixation was as described
797 below in "Immunofluorescence" section. Blocking steps included incubation in
798 1xPBS/0.1% Triton-X-100/0.1% BSA (PBS-T/BSA) for 2×15 minutes at room
799 temperature, in 10% normal goat serum for 1 hour at room temperature in a light-sealed
800 humid chamber, and in Duolink blocking buffer (Sigma-Aldrich) for 1 hour at 37°C in a
801 light-sealed humid chamber. Primary antibodies (see Table S3 for antibody information)
802 were diluted in PBS-T/BSA and incubated overnight at 4°C. Samples were then
803 incubated with Duolink PLA probes (see Table S3) for 1 hour at 37°C in a light-sealed
804 chamber. Next, slides were incubated in a light-sealed humid chamber for 30 minutes at
805 37°C for ligation, and then for 100 minutes at 37°C for amplification before finally being
806 mounted with Duolink Mounting medium with DAPI (Sigma-Aldrich). Images were
807 acquired using Zeiss 880 confocal microscope, and the ImageJ "Analyze Particles"
808 plug-in was used to quantify PLA foci in germline images.

809

810 **RNA extraction and RT-qPCR**

811 *C. elegans* were synchronized by bleaching and hatched L1 larvae were plated on
812 NNGM plates with OP50 bacteria, grown at 20°C, and collected after 72 hours. 200-400
813 worms were collected per biological replicate and stored in Trizol (Invitrogen) at -80˚C.
814 Total RNA was extracted using either Monarch Total RNA Miniprep Kit (New England
815 Biolabs) or Direct-zol™ RNA MiniPrep kit (Zymo Research) as per manufacturers'
816 protocols. RNA concentration was measured using Qubit (Thermo Fisher). cDNA was
817 synthesized using the SuperScript™ IV reverse transcriptase (Invitrogen) using 300 ng
818 RNA template per each 20 µL cDNA synthesis reaction. Quantitative PCR reactions
819 were performed in technical triplicates per each input cDNA using iQ SYBR® Green
820 Supermix (Bio-Rad). Primers for all targets were as previously described: *act-1* and *fbf-*
821 *2* (Chauve et al., 2020), *unc-54* (Wang et al., 2020), and *fbf-1* (Voronina and Seydoux,
822 2010), all primers are listed in Table S4. Abundance of each mRNA in *csn(lf)* mutant
823 relative to the wild type was calculated using comparative ΔΔCt method (Plaffl, 2001)

824 with actin *act-1* as a reference gene. After mRNA abundance of each tested gene was
825 normalized to *act-1*, the fold change values from replicates were averaged.

826

827 **Immunofluorescence**

828 Adult *C. elegans* hermaphrodites were washed in M9 and germlines were dissected on
829 poly-L-lysine treated slides, flash frozen, and fixed for 1 minute in 100% methanol (-
830 20°C) followed by 5 minutes in 2% paraformaldehyde/100 mM K_2HPO_4 (pH 6) at room
831 temperature. The samples were then blocked in PBS-T/BSA for 30 minutes at room
832 temperature. Next, samples were incubated with primary antibody (see Table S3 for
833 antibody information) diluted in PBS-T/BSA overnight at 4°C. Samples were then
834 washed with PBS-T/BSA three times for 10 minutes per wash, before incubating with
835 secondary antibody diluted in PBS-T/BSA for 2 hours at room temperature in a dark
836 humid chamber. Samples were washed again three times for 10 minutes per wash
837 before adding 10 µL Vectashield® with DAPI (Vector Laboratories) and cover-slipping.
838 Images were acquired with a Leica DFC300G camera attached to a Leica DM5500B
839 microscope with a 40x LP FLUOTAR NA1.3 objective using LAS X software (Leica) and
840 stitched together using Adobe Photoshop CS3.

841

842 **Fluorescence quantitation**

843 To analyze PUF-3 levels in *csn-5(lf)* and FBF levels in *csn-5(lf)* mutant treated with
844 control or *ned-8(RNAi)*, adult *C. elegans* hermaphrodites were washed in M9, germlines
845 were dissected, and slides were processed as described above under the
846 "Immunofluorescence" section. Z-stack images spanning the thickness of germline were
847 taken under identical conditions across all samples in each experiment. PUF-3 and FBF
848 protein levels within the SPC zone were analyzed using Fiji/ImageJ as previously
849 described with some modifications (Brenner and Schedl, 2016; Haupt et al., 2019). On
850 the maximum intensity projection generated from each z-stack, the segmented line
851 (width set to 45) tool was used to draw a freehand line from the distal tip through the
852 length of the SPC zone (as indicated by co-staining with REC-8 antibody, Hansen et al.,

853 2004 or DNA morphology with DAPI) that bisected the gonad. Next, pixel intensity data
854 for both V5 and FBF-1 channels were obtained using “Plot Profile” to generate raw
855 intensity curves. To adjust for non-specific background staining, we subtracted the
856 average intensity of the respective negative controls (N2 for V5::PUF-3 analysis and *fbf-*
857 *1(ok91)* for FBF-1 and V5::FBF-2 analysis) from expression curves of each respective
858 genotype. The maximum background-subtracted values for each wild type and mutant
859 germline were determined and used in further analysis. The maximum values of wild
860 type germlines were averaged, and the average value was used for normalization of all
861 values to set the wild type levels to 1. To better visualize 3xV5::PUF-3 expression in the
862 SPC zone for Fig. 4L, M, images were acquired using a Zeiss 880 confocal microscope
863 under identical conditions and V5 intensity was adjusted equally in Adobe Photoshop
864 CS3 for *3xv5::puf-3* and *csn-5(lf) 3xv5::puf-3* genetic backgrounds.

865

866 **Germline SPC counts**

867 *C. elegans* were synchronized by bleaching and hatched L1 larvae were plated on
868 NNGM plates with OP50 bacteria, grown at 20°C, and harvested 24 hours post-L4.
869 Gonads were dissected and stained for progenitor cell marker REC-8 (Hansen et al.,
870 2004), and the number of stem and progenitor cells was measured by counting the total
871 number of cells positive for REC-8 staining using Cell Counter plug-in in Fiji (Schindelin
872 et al., 2012) or Imaris 9.9 software.

873

874 **EdU labeling**

875 EdU labeling was performed as previously described with some modifications (Wang et
876 al., 2020). EdU bacterial plates were prepared by diluting an overnight culture of
877 thymine deficient MG1693 *E. coli* (The Coli Genetic Stock Center; Yale University) 1/25
878 in 1% glucose, 1 mM $MgSO_4$, 5 µg/mL thymine, 6 µM thymidine, and 20 µM EdU in M9.
879 This culture was grown at 37°C for 24 hours, pelleted by centrifugation, resuspended in
880 10 mL M9 and plated on NNGM plates. Worm strains were synchronized by bleaching
881 and hatched L1 larvae were plated on NNGM plates with OP50 bacteria, grown at 20°C

882 for 72 hours to reach young adult stage when they were exposed to EdU-labeled
883 bacteria for either 4 or 14 hours (Fig. 5C, D and E-G, respectively). After feeding for the
884 specified time, worms were dissected for immunostaining as described in
885 "Immunofluorescence" section above. After incubation with secondary antibody (see
886 Table S3 for antibody information), slides were washed four times for 15 minutes per
887 wash in PBS-T/BSA. Next, the Click-iT reaction was performed according to
888 manufacturer instructions with the exception that two 30-minute Click-iT reactions were
889 performed to increase the signal of the Alexa 488 dye. After incubation with the second
890 Click-iT reaction, slides were washed four times for 15 minutes per wash in PBS-T/BSA
891 before adding 10 µL Vectashield® with DAPI (Vector Laboratories) and cover-slipping.

892

893 **Phenotypic analysis**

894 For germline sex analysis (Fig. 6), *C. elegans* were synchronized by bleaching and
895 hatched L1 larvae were plated on NNGM plates with OP50 bacteria, grown at 20°C, and
896 harvested after 24 hours post-L4. Gonads were dissected, stained for DNA with DAPI,
897 and scored for abnormal oocytes (defined as <3 oocytes per germline, uncondensed
898 chromosomes, endomitotic oocytes, or increased number of DAPI spots indicating
899 achiasmatic chromosomes), sperm only, and failure of gamete formation.

900 For scoring fertility in *csn-5(ok1064)* mutant strains (Table 1), *C. elegans* were
901 synchronized by bleaching and hatched L1 larvae were plated on NNGM plates with
902 OP50 bacteria and grown at 20°C for 96 hours before scoring fertility using a dissecting
903 microscope. "Fertile" was classified by presence of embryos in the uteri and lack of
904 embryos was classified as sterile.

905

906 **RNAi treatment**

907 For RNAi, two knockdown methods were utilized. Feeding RNAi was utilized for *pbs-6*
908 and *fbf-2* RNAi constructs in pL4440 (Kamath and Ahringer, 2003). Empty vector
909 pL4440 was used as a control in all RNAi experiments. All RNAi constructs were

910 verified by sequencing and transformed into HT115 (DE3) *Escherichia coli*. Three
911 colonies of freshly transformed RNAi plasmids were combined for growth in LB/75
912 µg/mL carbenicillin media for 4 hours, and induced with 5 mM IPTG for 1-2 hours at
913 37°C. RNAi plates (NNGM containing 100 µg/mL carbenicillin and 0.4 mM IPTG) were
914 seeded with the pelleted cells. Synchronously hatched L1 larvae were plated directly on
915 RNAi plates, grown at 24°C, and collected for analysis after reaching adulthood.

916 Soaking RNAi for *ned-8* was performed as described by Yoon et al., 2012 with some
917 modifications. Templates for *in vitro* transcription of *ned-8* flanked by T7 promoter
918 sequences were amplified via PCR from RNAi constructs in pL4440 (Source BioScience
919 RNAi library; Kamath and Ahringer, 2003). Templates were then transcribed into dsRNA
920 *in vitro* using a T7 MEGAscript® Kit (Invitrogen) per manufacturer's instructions at the
921 100 µL scale. dsRNA was then recovered using an RNA Cleanup Kit (New England
922 Biolabs) per manufacturer's instructions. Synchronously hatched L1 larvae (200-400)
923 were then suspended in soaking buffer containing 2.5X M9, 30 mM spermidine, and
924 0.5% gelatin with 1 µg/µL dsRNA for 48 hours at 20°C. Larvae were then plated on
925 OP50 plates for another 72 hours, and were collected for analysis after reaching
926 adulthood.

927

928 **Acknowledgements:**

929 We thank members of the Voronina laboratory for helpful discussions. All research was
930 performed at the University of Montana. Several nematode strains were provided by the
931 *Caenorhabditis* Genetics Center, funded by the National Institutes of Health (NIH) (grant
932 P40OD010440). *csn* knockout strains were generated by the *C. elegans* Reverse
933 Genetics Core Facility at the University of British Columbia and Oklahoma Medical
934 Research Foundation, both part of the international *C. elegans* Gene Knockout
935 Consortium (Barstead et al., 2012). Confocal microscopy was performed in the
936 University of Montana BioSpectroscopy Core Research Laboratory operated with
937 support from NIH awards P20GM103546 and S10OD021806. We are grateful to
938 Gabriella Weiss for help with strain generation, Nicholas Day for assistance with
939 Western blot, and James Bosco, Ella Baumgarten, and Polash Biswas for help with

cloning. We thank Beverly Piggott and Isabella Maag for sharing, and instruction, of Imaris cell counting software.

Author Contributions:

E.O. contributed to all Figures, participated in study design, manuscript drafting and editing. M.E. provided strains, constructs, and experimental data related to Fig. 2, 4-6, S1, S2, and S6. X.W. provided constructs and contributed to Fig. 1, 2, 4, and Table S1. M.T., K.J., and D.C. contributed strains and experimental data related to Fig. 5-7, S4, S5, and Table 1. E.V. contributed to generation of strains and plasmids, provided general study design, coordination, manuscript drafting and editing. All authors made manuscript revisions and approved the manuscript.

Funding:

This work was supported by NIH grants R01GM109053 to E.V., P20GM103546 (S. Sprang, PI; E.V. Pilot Project PI), and P20GM103474 (B. Bothner, PI; E.V. infrastructure support awardee), and Toelle-Bekken Family Memorial Fund Award to E.O. The funders had no role in the study design, data collection and analysis, decision to publish, or preparation of the manuscript.

Competing interests:

The authors declare no competing or financial interests.

Data availability

This study did not generate large datasets or codes, but raw data/images are available upon request.

965 **References:**

966 1. Ariz, M., Mainpal, R., and Subramaniam, K. (2009). *C. elegans* RNA-binding
967 proteins PUF-8 and MEX-3 function redundantly to promote germline stem cell
968 mitosis. Dev Biol, *326*, 295-304.
969 2. Austin, J., and Kimble, J. (1987). *glp-1* is required in the germ line for regulation
970 of the decision between mitosis and meiosis in *C. elegans*. Cell, *51*, 589–599.
971 3. Bae, M.K., Ahn, M.Y., Jeong, J.W., Bae, M.H., Lee, Y.M., Bae, S.K., Park, J.W.,
972 Kim, K.R., and Kim, K.W. (2002). Jab1 interacts directly with HIF-1alpha and
973 regulates its stability. J Biol Chem, *277*, 9–12.
974 4. Barstead, R., Moulder, G., Cobb, B., Frazee, S., Henthorn, D., Holmes, J.,
975 Jerebie, D., Landsdale, M., Osborn, J., Pritchett, C. et al. (2012). Large-scale
976 screening for targeted knockouts in the *Caenorhabditis elegans* genome. G3
977 (Bethesda), *2*, 1415–1425.
978 5. Belfiore, M., Pugnale, P., Saudan, Z., and Puoti, A. (2004). Roles of the *C.*
979 *elegans* cyclophilin-like protein MOG-1 in MEP-1 binding and germline fates.
980 Development, *131,* 2935-2945.
981 6. Bemis, L., Chan, D.A., Finkielstein, C.V., Qi, L., Sutphin, P.D., Chen, X.,
982 Stenmark, K., Giaccia, A.J., and Zundel, W. (2004). Distinct aerobic and hypoxic
983 mechanisms of HIF-alpha regulation by CSN5. Genes Dev, *18*, 739–744.
984 7. Bernstein, D., Hook, B., Hajarnavis, A., Opperman, L., and Wickens, M. (2005).
985 Binding specificity and mRNA targets of a *C. elegans* PUF protein, FBF-1. RNA,
986 *11*, 447-458.
987 8. Berry, L.W., Westlund, B., and Schedl, T. (1997). Germ-line tumor formation
988 caused by activation of *glp-1*, a *Caenorhabditis elegans* member of the *Notch*
989 family of receptors. Development, *124*, 925–936.
990 9. Birol, M., Enchev, R.I., Padilla, A., Stengel, F., Aebersold, R., Betzi, S., Yang, Y.,
991 Hoh, F., Peter, M., Dumas, C. et al. (2014). Structural and biochemical
992 characterization of the Cop9 signalosome CSN5/CSN6 heterodimer. PLoS One,
993 *9*, e105688.

994 10. Boh, B.K., Smith, P.G., and Hagen, T. (2011). Neddylation-induced
995 conformational control regulates cullin RING ligase activity *in vivo*. J Mol Biol,
996 *409*,136-145.
997 11. Brenner, J.L., Jyo, E.M., Mohammad, A., Fox, P., Jones, V., Mardis, E., Schedl,
998 T., and Maine, E.M. (2022). TRIM-NHL protein, NHL-2, modulates cell fate
999 choices in the *C. elegans* germ line. Dev Biol, *491*, 43-55.
1000 12. Brenner, J.L., and Schedl, T. (2016). Germline stem cell differentiation entails
1001 regional control of cell fate regulator GLD-1 in *Caenorhabditis elegans*. Genetics,
1002 *202*, 1085-1103.
1003 13. Brenner, S. (1974). The genetics of *Caenorhabditis elegans*. Genetics, *77*, 71–
1004 94.
1005 14. Brockway, H., Balukoff, N., Dean, M., Alleva, B., and Smolikove, S. (2014). The
1006 CSN/COP9 signalosome regulates synaptonemal complex assembly during
1007 meiotic prophase I of *Caenorhabditis elegans*. PLoS Genet, *10*, e1004757.
1008 15. Buck, S.H., Chiu, D., and Saito, R.M. (2009). The cyclin-dependent kinase
1009 inhibitors, *cki-1* and *cki-2*, act in overlapping but distinct pathways to control cell
1010 cycle quiescence during *C. elegans* development. Cell Cycle, *8*, 2613–2620.
1011 16. Chamovitz, D.A. (2009). Revisiting the COP9 signalosome as a transcriptional
1012 regulator. EMBO Rep, *10*, 352–358.
1013 17. Chamovitz, D.A., Wei, N., Osterlund, M.T., von Arnim, A.G., Staub, J.M., Matsui,
1014 M., and Deng, X.W. (1996). The COP9 complex, a novel multisubunit nuclear
1015 regulator involved in light control of a plant developmental switch. Cell, *86*, 115–
1016 121.
1017 18. Chauve, L., Le Pen, J., Hodge, F., Todtenhaupt, P., Biggins, L., Miska, E.A.,
1018 Andrews, S., and Casanueva, O. (2020). High-Throughput Quantitative RT-PCR
1019 in Single and Bulk C. elegans Samples Using Nanofluidic Technology. J Vis
1020 Exp, *159*, e61132
1021 19. Chen, J., Mohammad, A., Pazdernik, N., Huang, H., Bowman, B., Tycksen, E.,
1022 and Schedl, T. (2020). GLP-1 Notch-LAG-1 CSL control of the germline stem cell
1023 fate is mediated by transcriptional targets *lst-1* and *sygl-1*. PLoS Genet, *16*,
1024 e1008650.

1025 20. Claret, F.X., Hibi, M., Dhut, S., Toda, T., and Karin, M. (1996). A new group of
1026 conserved coactivators that increase the specificity of AP-1 transcription factors.
1027 Nature, *383*, 453–457.
1028 21. Cope, G.A., Suh, G.S., Aravind, L., Schwarz, S.E., Zipursky, S.L., Koonin, E.V.,
1029 and Deshaies, R.J. (2002). Role of predicted metalloprotease motif of Jab1/Csn5
1030 in cleavage of Nedd8 from Cul1. Science, *298*, 608–611.
1031 22. Crittenden, S.L., Bernstein, D.S., Bachorik, J.L., Thompson, B.E., Gallegos, M.,
1032 Petcherski, A.G., Moulder, G., Barstead, R., Wickens, M., and Kimble, J. (2002).
1033 A conserved RNA-binding protein controls germline stem cells in *Caenorhabditis*
1034 *elegans*. Nature, *417*, 660–663.
1035 23. Day, N.J., Wang, X., and Voronina, E. (2020). *In situ* detection of
1036 ribonucleoprotein complex assembly in the *C. elegans* germline using proximity
1037 ligation assay. J Vise Exp, *159*, e60982.
1038 24. Demarco, R.S., Stack, B.J., Tang, A.M., Voog, J., Sandall, S.L., Southall, T.D.,
1039 Brand, A.H., and Jones, D.L. (2022). Escargot controls somatic stem cell
1040 maintenance through the attenuation of the insulin receptor pathway in
1041 *Drosophila*. Cell Rep, *39*, 110679.
1042 25. Dessau, M., Halimi, Y., Erez, T., Chomsky-Hecht, O., Chamovitz, D.A., and
1043 Hirsch, J.A. (2008). The *Arabidopsis* COP9 signalosome subunit 7 is a model
1044 PCI domain protein with subdomains involved in COP9 signalosome assembly.
1045 Plant Cell, *20*, 2815–2834.
1046 26. Dickinson, D.J., Ward, J.D., Reiner, D.J., and Goldstein, B. (2013). Engineering
1047 the *Caenorhabditis elegans* genome using Cas9-triggered homologous
1048 recombination. Nat Methods, *10*, 1028–1034.
1049 27. Doronkin, S., Djagaeva, I., and Beckendorf, S.K. (2003). The COP9 signalosome
1050 promotes degradation of Cyclin E during early *Drosophila* oogenesis. Dev Cell, *4*,
1051 699–710.
1052 28. Duda, D.M., Borg, L.A., Scott, D.C., Hunt, H.W., Hammel, M., and Schulman,
1053 B.A. (2008). Structural insights into NEDD8 activation of cullin-RING ligases:
1054 conformational control of conjugation. Cell, *134*, 995-1006.

1055 29. Echalier, A., Pan, Y., Birol, M., Tavernier, N., Pintard, L., Hoh, F., Ebel, C.,
1056 Galophe, N., Claret, F.X., and Dumas, C. (2013). Insights into the regulation of
1057 the human COP9 signalosome catalytic subunit, CSN5/Jab1. Proc Natl Acad Sci
1058 U S A, *110*, 1273–1278.
1059 30. Eckmann, C.R., Kraemer, B., Wickens, M., and Kimble, J. (2002). GLD-3, a
1060 bicaudal-C homolog that inhibits FBF to control germline sex determination in *C.*
1061 *elegans*. Dev Cell, *3*, 697-710.
1062 31. Ellenbecker, M., Osterli, E., Wang, X., Day, N.J., Baumgarten, E., Hickey, B., and
1063 Voronina, E. (2019). Dynein light chain DLC-1 facilitates the function of the
1064 germline cell fate regulator GLD-1 in *Caenorhabditis elegans*. Genetics, *211*,
1065 665-681.
1066 32. Ellis, R.E. (2022). Sex determination in nematode germ cells. Sex Dev, 1-18.
1067 33. Enchev, R.I., Scott, D.C., da Fonseca, P.C., Schreiber, A., Monda, J.K.,
1068 Schulman, B.A., Peter, M., and Morris, E.P. (2012). Structural basis for a
1069 reciprocal regulation between SCF and CSN. Cell Rep, *2*, 616–627.
1070 34. Fox, P.M., Vought, V.E., Hanazawa, M., Lee, M.H., Maine, E.M., and Schedl, T.
1071 (2011). Cyclin E and CDK-2 regulate proliferative cell fate and cell cycle
1072 progression in the *C. elegans* germline. Development, *138*, 2223-2234.
1073 *35.* Friend, K., Campbell, Z.T., Cooke, A., Kroll-Conner, P., Wickens, M.P., and
1074 Kimble, J. (2012). A conserved PUF-Ago-eIF1A complex attenuates translational
1075 elongation. Nat Struct Mol Biol, *19*, 176-183.
1076 36. Frøkjaer-Jensen, C., Davis, M.W., Hopkins, C.E., Newman, B.J., Thummel, J.M.,
1077 Olesen, S.P., Grunnet, M., and Jorgensen, E.M. (2008). Single-copy insertion of
1078 transgenes in *Caenorhabditis elegans*. Nat Genet, *40*, 1375–1383.
1079 37. Gor, R., Sampath, S.S., Lazer, L.M., and Ramalingam, S. (2021). RNA binding
1080 protein PUM1 promotes colon cancer cell proliferation and migration. Int J Biol
1081 Macromol, *174*, 549–561.
1082 38. Groisman, R., Polanowska, J., Kuraoka, I., Sawada, J., Saijo, M., Drapkin, R.,
1083 Kisselev, A.F., Tanaka, K., and Nakatani, Y. (2003). The ubiquitin ligase activity
1084 in the DDB2 and CSA complexes is differentially regulated by the COP9
1085 signalosome in response to DNA damage. Cell, *113*, 357–367.

1086 39. Guan, X., Chen, S., Liu, Y., Wang, L.L., Zhao, Y., and Zong, Z.H. (2018). PUM1
1087 promotes ovarian cancer proliferation, migration and invasion. Biochem Biophys
1088 Res Commun, *497*, 313–318.
1089 40. Hallstrom, T.C., and Nevins, J.R. (2006). Jab1 is a specificity factor for E2F1-
1090 induced apoptosis. Genes Dev, *20*, 613-623.
1091 41. Hansen, D., Hubbard, E.J., and Schedl, T. (2004). Multi-pathway control of the
1092 proliferation versus meiotic development decision in the *Caenorhabditis elegans*
1093 germline. Dev Biol, *268*, 342–357.
1094 42. Hansen, D., and Schedl, T. (2013). Stem cell proliferation versus meiotic fate
1095 decision in *Caenorhabditis elegans*. Adv Exp Med Biol, *757*, 71-99.
1096 43. Haupt, K.A., Enright, A.L., Ferdous, A.S., Kershner, A.M., Shin, H., Wickens, M.,
1097 and Kimble, J. (2019). The molecular basis of LST-1 self-renewal activity and its
1098 control of stem cell pool size. Development, *146*, dev181644.
1099 *44.* Haupt, K.A., Law, K.T., Enright, A.L., Kanzler, C.R., Shin, H., Wickens, M., and
1100 Kimble, J. (2020). A PUF hub drives self-renewal in *Caenorhabditis elegans*
1101 germline stem cells. Genetics, *214*, 147-161.
1102 45. Hetfeld, B.K., Helfrich, A., Kapelari, B., Scheel, H., Hofmann, K., Guterman, A.,
1103 Glickman, M., Schade, R., Kloetzel, P.M., and Dubiel, W. (2005). The zinc finger
1104 of the CSN-associated deubiquitinating enzyme USP15 is essential to rescue the
1105 E3 ligase Rbx1. Curr Biol, *15*, 1217–1221.
1106 46. Hofmann, K., and Bucher, P. (1998). The PCI domain: a common theme in three
1107 multiprotein complexes. Trends Biochem Sci, *23*, 204–205.
1108 47. Hubbard, E.J. (2007). *Caenorhabditis elegans* germ line: a model for stem cell
1109 biology. Dev Dyn, *236*, 3343–3357.
1110 48. James, P., Halladay, J., and Craig, E.A. (1996). Genomic libraries and a host
1111 strain designed for highly efficient two-hybrid selection in yeast. Genetics, *144*,
1112 1425–1436.
1113 49. Jones, A.R., Francis, R., and Schedl, T. (1996). GLD-1, a cytoplasmic protein
1114 essential for oocyte differentiation, shows stage- and sex-specific expression
1115 during *Caenorhabditis elegans* germline development. Dev Biol, *180*, 165-183.

1116 50. Kalchhauser, I., Farley, B.M., Pauli, S., Ryder, S.P., and Ciosk, R. (2011). FBF
1117 represses the Cip/Kip cell-cycle inhibitor CKI-2 to promote self-renewal of
1118 germline stem cells in *C. elegans*. EMBO J, *30*, 3823–3829.
1119 51. Kamath, R.S., and Ahringer, J. (2003). Genome-wide RNAi screening in
1120 *Caenorhabditis elegans*. Methods, *30*, 313–321.
1121 52. Kimble, J., and Crittenden, S.L. (2007). Controls of germline stem cells, entry into
1122 meiosis, and the sperm/oocyte decision in *Caenorhabditis elegans*. Annu Rev
1123 Cell Dev Biol, *23*, 405–433.
1124 53. Kimble, J.E., and White, J.G. (1981). On the control of germ cell development in
1125 *Caenorhabditis elegans*. Dev Biol, *81*, 208–219.
1126 54. Kocsisova, Z., Mohammad, A., Kornfeld, K., and Schedl, T. (2018). Cell cycle
1127 analysis in the *C. elegans* germline with thymidine analog EdU. J Vis Exp, *140*,
1128 e58339.
1129 55. Konishi, T., Uodome, N., and Sugimoto, A. (2008). The *Caenorhabditis elegans*
1130 DDX-23, a homolog of yeast splicing factor PRP28, is required for the sperm-
1131 oocyte switch and differentiation of various cell types. Dev Dyn, *237*, 2267-2277.
1132 *56.* Kraemer, B., Crittenden, S., Gallegos, M., Moulder, G., Barstead, R., Kimble, J.,
1133 and Wickens, M. (1999). NANOS-3 and FBF proteins physically interact to
1134 control the sperm-oocyte switch in *Caenorhabditis elegans*. Curr Biol, *9*, 1009-
1135 1018.
1136 57. Kumsta, C., and Hansen, M. (2012). *C. elegans rrf-1* mutations maintain RNAi
1137 efficiency in the soma in addition to the germline. PLoS One, *7*, e35428.
1138 58. Lamont, L.B., Crittenden, S.L., Bernstein, D., Wickens, M., and Kimble, J. (2004).
1139 FBF-1 and FBF-2 regulate the size of the mitotic region in *C. elegans* germline.
1140 Dev Cell, *7*, 697-707.
1141 59. Lee, C., Sorensen, E.B., Lynch, T.R., and Kimble, J. (2016). *C. elegans* GLP-
1142 1/Notch activates transcription in a probability gradient across the germline stem
1143 cell pool. eLife, *5*, e18370.
1144 60. Lee, M.H., Zhao, R., Phan, L., and Yeung, S.C. (2011). Roles of COP9
1145 signalosome in cancer. Cell Cycle, *10*, 3057–3066.

1146 61. Lim, S.O., Li, C.W., Xia, W., Cha, J.H., Chan, L.C., Wu, Y., Chang, S.S., Lin,
1147 W.C., Hsu, J.M., Hsu, Y.H. et al. (2016). Deubiquitination and Stabilization of PD-
1148 L1 by CSN5. Cancer Cell, *30*, 925–939.
1149 62. Lingaraju, G.M., Bunker, R.D., Cavadini, S., Hess, D., Hassiepen, U., Renatus,
1150 M., Fischer, E.S., and Thomä, N.H. (2014). Crystal structure of the human COP9
1151 signalosome. Nature, *512*, 161–165.
1152 63. Liu, Y., Shah, S.V., Xiang, X., Wang, J., Deng, Z.B., Liu, C., Zhang, L., Wu, J.,
1153 Edmonds, T., Jambor, C. et al. (2009). COP9-associated CSN5 regulates
1154 exosomal protein deubiquitination and sorting. Am J Pathol, *174*, 1415–1425.
1155 64. Liu, C., Yao, Z., Wang, J., Zhang, W., Yang, Y., Zhang, Y., Qu, X., Zhu, Y., Zou,
1156 J., Peng, S. et al. (2020). Macrophage-derived CCL5 facilitates immune escape
1157 of colorectal cancer cells via the p65/STAT3-CSN5-PD-L1 pathway. Cell Death
1158 Differ, *27*, 1765–1781.
1159 *65.* Llamas, E., Alirzayeva, H., Loureiro, R., and Vilchez, D. (2020). The intrinsic
1160 proteostasis network of stem cells. Curr Opin Cell Biol, *67*, 46-55.
1161 66. Lyapina, S., Cope, G., Shevchenko, A., Serino, G., Tsuge, T., Zhou, C., Wolf,
1162 D.A., Wei, N., Shevchenko, A., and Deshaies, R.J. (2001). Promotion of NEDD-
1163 CUL1 conjugate cleavage by COP9 signalosome. Science, *292*, 1382–1385.
1164 67. Lykke-Andersen, K., Schaefer, L., Menon, S., Deng, X.W., Miller, J.B., and Wei,
1165 N. (2003). Disruption of COP9 signalosome Csn2 subunit in mice causes
1166 deficient cell proliferation, accumulation of p53 and cyclin E, and early embryonic
1167 death. Mol Cell Biol, *23*, 6790-6797.
1168 68. Ma, X.L., Xu, M., and Jiang, T. (2014). Crystal structure of the human CSN6
1169 MPN domain. Biochem Biophys Res Commun, *453*, 25-30.
1170 *69.* Mantina, P., MacDonald, L., Kulaga, A., Zhao, L., and Hansen, D. (2009). A
1171 mutation in *teg-4,* which encodes a protein homologous to the SAP130 pre-
1172 mRNA splicing factor, disrupts the balance between proliferation and
1173 differentiation in the *C. elegans* germ line. Mech Dev, *126*, 417-429.
1174 70. Marnik, E.A., Fuqua, J.H., Sharp, C.S., Rochester, J.D., Xu, E.L., Holbrook, S.E.,
1175 and Updike, D.L. (2019). Germline maintenance through multifaceted activities of
1176 GLH/Vasa in *Caenorhabditis elegans* P granules. Genetics, *213*, 923-939.

1177 71. Merritt, C., and Seydoux, G. (2010). The Puf RNA-binding proteins FBF-1 and
1178 FBF-2 inhibit the expression of synaptonemal complex proteins in germline stem
1179 cells. Development, *137*, 1787-1798.
1180 72. Miller, R.K., Qadota, H., Stark, T.J., Mercer, K.B., Wortham, T.S., Anyanful, A.,
1181 and Benian, G.M. (2009). CSN-5, a component of the COP9 signalosome
1182 complex, regulates the levels of UNC-96 and UNC-98, two components of M-
1183 lines in *Caenorhabditis elegans* muscle. Mol Biol Cell, *20*, 3608–3616.
1184 73. Morgan, D. E., Crittenden, S. L., and Kimble, J. (2010). The *C. elegans* adult
1185 male germline: stem cells and sexual dimorphism. Dev Biol, *346*, 204-214.
1186 74. Morrison, S.J., Shah, N.M., and Anderson, D.J. (1997). Regulatory mechanisms
1187 in stem cell biology. Cell, *88*, 287–298.
1188 75. Oron, E., Mannervik, M., Rencus, S., Harari-Steinberg, O., Neuman-Silberberg,
1189 S., Segal, D., and Chamovitz, D.A. (2002). COP9 signalosome subunits 4 and 5
1190 regulate multiple pleiotropic pathways in *Drosophila melanogaster*. Development,
1191 *129*, 4399-4409.
1192 76. Orsborn, A.M., Li, W., McEwen, T.J., Mizuno, T., Kuzmin, E., Matsumoto, K., and
1193 Bennett, K.L. (2007). GLH-1, the *C. elegans* P granule protein, is controlled by
1194 the JNK KGB-1 and by the COP9 subunit CSN-5. Development, *134*, 3383–
1195 3392.
1196 77. Pan, L., Wang, S., Lu, T., Weng, C., Song, X., Park, J.K., Sun, J., Yang, Z., Yu,
1197 J., Tang, H., et al. (2014). Protein competition switches the function of COP9
1198 from self-renewal to differentiation. Nature, *514*, 233-236.
1199 78. Pazdernik, N., and Schedl, T. (2013). Introduction to germ cell development in
1200 *Caenorhabditis elegans*. Adv Exp Med Biol, *757*, 1–16.
1201 79. Peth, A., Berndt, C., Henke, W., and Dubiel, W. (2007). Downregulation of COP9
1202 signalosome subunits differentially affects the CSN complex and target protein
1203 stability. BMC Biochem, *8*, 27.
1204 80. Pfaffl, M.W. (2001). A new mathematical model for relative quantification in real-
1205 time RT-PCR. Nucleic Acids Res, *29*, e45.
1206 81. Pintard, L., Kurz, T., Glaser, S., Willis, J.H., Peter, M., and Bowerman, B. (2003).
1207 Neddylation and deneddylation of CUL-3 is required to target MEI-1/Katanin for

1208 degradation at the meiosis-to-mitosis transition in *C. elegans*. Curr Biol, *13*, 911–
1209 921.
1210 82. Prasad, A., Porter, D.F., Kroll-Conner, P.L., Mohanty, I., Ryan, A.R., Crittenden,
1211 S.L., Wickens, M., and Kimble, J. (2016). The PUF binding landscape in
1212 metazoan germ cells. RNA, *22*, 1026–1043.
1213 83. Puoti, A., and Kimble, J. (1999). The *Caenorhabditis elegans* sex determination
1214 gene *mog-1* encodes a member of the DEAH-Box protein family. Mol Cell Biol,
1215 *19*, 2189-2197.
1216 84. Puoti, A., and Kimble, J. (2000). The hermaphrodite sperm/oocyte switch
1217 requires the *Caenorhabditis elegans* homologs of PRP2 and PRP22. Proc Natl
1218 Acad Sci U S A, *97*, 3276-3281.
1219 85. Qin, N., Xu, D., Li, J., and Deng, X.W. (2020). COP9 signalosome: Discovery,
1220 conservation, activity, and function. J Integr Plant Biol, *62*, 90–103.
1221 86. Racher, H., and Hansen, D. (2012). PUF-8, a Pumilio homolog, inhibits the
1222 proliferative fate in the *Caenorhabditis elegans* germline. G3 (Bethesda), *2*,
1223 1197-1205.
1224 87. Saha, A., and Deshaies, R.J. (2008). Multimodal activation of the ubiquitin ligase
1225 SCF by Nedd8 conjugation. Mol Cell, *32*, 21-31.
1226 88. Samuels, T.J., Järvelin, A.I., Ish-Horowicz, D., and Davis, I. (2020). Imp/IGF2BP
1227 levels modulate individual neural stem cell growth and division through. eLife,
1228 *9*, e51529.
1229 89. Schindelin, J., Arganda-Carreras, I., Frise, E., Kaynig, V., Longair, M., Pietzsch,
1230 T., Preibisch, S., Rueden, C., Saalfeld, S., Schmid, B. et al. (2012). Fiji: an open-
1231 source platform for biological-image analysis. Nat Methods, *9*, 676–682.
1232 90. Shackleford, T.J., and Claret, F.X. (2010). JAB1/CSN5: a new player in cell cycle
1233 control and cancer. Cell Div, *5*, 26.
1234 91. Sharon, M., Mao, H., Boeri Erba, E., Stephens, E., Zheng, N., and Robinson,
1235 C.V. (2009). Symmetrical modularity of the COP9 signalosome complex
1236 suggests its multifunctionality. Structure, *17*, 31–40.
1237 92. Shi, P., Zhang, J., Li, X., Li, W., Li, H., and Fu, P. (2021). Long non-coding RNA
1238 NORAD inhibition upregulates microRNA-323a-3p to suppress tumorigenesis

1239 and development of breast cancer through the PUM1/eIF2 axis. Cell Cycle, *20*,
1240 1295–1307.
1241 93. Shin, H., Haupt, K.A., Kershner, A.M., Kroll-Conner, P., Wickens, M., and Kimble,
1242 J. (2017). SYGL-1 and LST-1 link niche signaling to PUF RNA repression for
1243 stem cell maintenance in *Caenorhabditis elegans*. PLoS Genet, *13*, e1007121.
1244 94. Sijen, T., Fleenor, J., Simmer, F., Thijssen, K.L., Parrish, S., Timmons, L.,
1245 Plasterk, R.H., and Fire, A. (2001). On the role of RNA amplification in dsRNA-
1246 triggered gene silencing. Cell, *107*, 465–476.
1247 95. Smialek, M.J., Ilaslan, E., Sajek, M.P., and Jaruzelska, J. (2021). Role of PUM
1248 RNA-binding proteins in cancer. Cancers (Basel), *13*, 129.
1249 96. Smith, P., Leung-Chiu, W.M., Montgomery, R., Orsborn, A., Kuznicki, K.,
1250 Gressman-Coberly, E., Mutapcic, L., and Bennett, K. (2002). The GLH proteins,
1251 *Caenorhabditis elegans* P granule components, associate with CSN-5 and KGB-
1252 1, proteins necessary for fertility, and with ZYX-1, a predicted cytoskeletal
1253 protein. Dev Biol, *251*, 333–347.
1254 97. Söderberg, O., Leuchowius, K.J., Gullberg, M., Jarvius, M., Weibrecht, I.,
1255 Larsson, L.G., and Landeregren, U. (2008). Characterizing proteins and their
1256 interactions in cells and tissues using the *in situ* proximity ligation assay.
1257 Methods, *45*, 227-232.
1258 98. Spassov, D.S., and Jurecic, R. (2002). Cloning and comparative sequence
1259 analysis of PUM1 and PUM2 genes, human members of the Pumilio family of
1260 RNA-binding proteins. Gene, *299*, 195-204.
1261 99. Spassov, D.S., and Jurecic, R. (2003). The PUF family of RNA-binding proteins,
1262 does evolutionarily conserved structure equal conserved function? IUBMB Life,
1263 *55*, 359-366.
1264 100. Spike, C.A., Tsukamoto, T., and Greenstein, D. (2022). Ubiquitin ligases
1265 and a processive proteasome protein clearance during the oocyte-to-embryo
1266 transition in *Caenorhabditis elegans*. Genetics, *221*, iyac051.
1267 101. Starostina, N.G., Lim, J., Schvarzstein, M., Wells, L., Spence, A.M., and
1268 Kipreos, E.T. (2007). A CUL-2 ubiquitin ligase containing three FEM proteins

1269 degrades TRA-1 to regulate *C. elegans* sex determination. Dev Cell, *13*, 127-
1270 139.
1271 102. Suh, N., Crittenden, S.L., Goldstrohm, A., Hook, B., Thompson, B.,
1272 Wickens, M., and Kimble, J. (2009). FBF and its dual control of *gld-1* expression
1273 in the *Caenorhabditis elegans* germline. Genetics, *181*, 1249–1260.
1274 103. Tomoda, K., Kubota, Y., and Kato, J. (1999). Degradation of the cyclin-
1275 dependent-kinase inhibitor p27Kip1 is instigated by Jab1. Nature, *398*, 160–165.
1276 104. Vilchez, D., Simic, M.S., and Dillin, A. (2014). Proteostasis and aging of
1277 stem cells. Trends Cell Biol, *24*, 161-170.
1278 105. Vogiatzoglou, A.P., Moretto, F., Makkou, M., Papamatheakis, J., and
1279 Kretsovali, A. (2022). Promyelocytic leukemia protein (PML) and stem cells: from
1280 cancer to pluripotency. Int J Dev Biol, *66*, 85–95.
1281 106. Voronina, E., and Greenstein, D. (2016). Germ cell fate determination in
1282 *C. elegans*. In eLS, John Wiley & Sons, Ltd: Chichester 1-8.
1283 107. Voronina, E., and Seydoux, G. (2010). The *C. elegans* homolog of
1284 nucleoporin Nup98 is required for the integrity and function of germline P
1285 granules. Development, *137*, 1441–1450.
1286 108. Voronina, E., Paix, A., and Seydoux, G. (2012). The P granule component
1287 PGL-1 promotes the localization and silencing activity of the PUF protein FBF-2
1288 in germline stem cells. Development, *139*, 3732–3740.
1289 *109.* Wang, C., Wilson-Berry, L., Schedl, T., and Hansen, D. (2012). TEG-1
1290 CD2BP2 regulates stem cell proliferation and sex determination in the *C. elegans*
1291 germ line and physically interacts with the UAF-1 U2AF65 splicing factor. Dev
1292 Dyn, *241*, 505-521.
1293 110. Wang, X., and Voronina, E. (2020). Diverse roles of PUF proteins in
1294 germline stem and progenitor cell development in *C. elegans*. Front Cell Dev
1295 Biol, *8*, 29.
1296 111. Wang, X., Ellenbecker, M., Hickey, B., Day, N.J., Osterli, E., Terzo, M.,
1297 and Voronina, E. (2020). Antagonistic control of *Caenorhabditis elegans* germline
1298 stem cell proliferation and differentiation by PUF proteins FBF-1and FBF-2. eLife,
1299 *9*, e52788.

1300 112. Wang, X., Olson, J.R., Rasoloson, D., Ellenbecker, M., Bailey, J., and
1301 Voronina, E. (2016). Dynein light chain DLC-1 promotes localization and function
1302 of the PUF protein FBF-2 in germline progenitor cells. Development, *143*, 4643–
1303 4653.
1304 113. Wee, S., Geyer, R.K., Toda, T., and Wolf, D.A. (2005). CSN facilitates
1305 Cullin-RING ubiquitin ligase function by counteracting autocatalytic adapter
1306 instability. Nat Cell Biol, *7*, 387–391.
1307 114. Wei, N., and Deng, X.W. (1992). COP9: a new genetic locus involved in
1308 light-regulated development and gene expression in *Arabidopsis*. Plant Cell, *4*,
1309 1507–1518.
1310 115. Wei, N., Chamovitz, D.A., and Deng, X.W. (1994). *Arabidopsis* COP9 is a
1311 component of a novel signaling complex mediating light control of development.
1312 Cell, *78*, 117–124.
1313 116. Wei, N., Serino, G., and Deng, X.W. (2008). The COP9 signalosome:
1314 more than a protease. Trends Biochem Sci, *33*, 592–600.
1315 117. Wickens, M., Bernstein, D.S., Kimble, J., and Parker, R. (2002). A PUF
1316 family portrait: 3'UTR regulation as a way of life. Trends Genet, *18*, 150–157.
1317 118. Wu, J.T., Lin, H.C., Hu, Y.C., and Chien, C.T. (2005). Neddylation and
1318 deneddylation regulate Cul1 and Cul3 protein accumulation. Nat Cell Biol, *7*,
1319 1014–1020.
1320 119. Wu, Y., Deng, J., Rychahou, P.G., Qiu, S., Evers, B.M., and Zhou, B.P.
1321 (2009). Stabilization of snail by NF-kappaB is required for inflammation-induced
1322 cell migration and invasion. Cancer Cell, *15*, 416-428.
1323 120. Yang, X., Menon, S., Lykke-Andersen, K., Tsuge, T., Xiao, D., Wang, X.,
1324 Rodriguez-Suarez, R.J., Zhang, H., and Wei, N. (2002). The COP9 signalosome
1325 inhibits p27(kip1) degradation and impedes G1-S phase progression via
1326 deneddylation of SCF Cul1. Curr Biol, *12*, 667-672.
1327 121. Yoon, S., Kawasaki, I., and Shim, Y.H. (2012). CDC-25.1 controls the rate
1328 of germline mitotic cell cycle by counteracting WEE-1.3 and by positively
1329 regulating CDK-1 in *Caenorhabditis elegans*. Cell Cycle, *11*, 1354-1363.

1330 122. Yoshida, A., Yoneda-Kato, N., and Kato, J.Y. (2013). CSN5 specifically
1331 interacts with CDK2 and controls senescence in a cytoplasmic cyclin E-mediated
1332 manner. Sci Rep, *3*, 1054.
1333 123. Yun, J., Tomida, A., Andoh, T., and Tsuruo, T. (2004). Interaction between
1334 glucose-regulated destruction domain if DNA topoisomerase IIα and MPN
1335 domain of Jab1/CSN5. J Biol Chem, *279*, 31296-31303.
1336 124. Zanetti, S., Meola, M., Bochud, A., and Puoti, A. (2011). Role of the *C.*
1337 *elegans* U2 snRNP protein MOG-2 in sex determination, meiosis, and splice site
1338 selection. Dev Biol, *354*, 232-241.
1339 125. Zhang, B., Gallegos, M., Puoti, A., Durkin, E., Fields, S., Kimble, J., and
1340 Wickens, M.P. (1997). A conserved RNA-binding protein that regulates sexual
1341 fates in the *C. elegans* hermaphrodite germ line. Nature, *390*, 477–484.
1342 126. Zhang, H., Gao, Z.Q., Wang, W.J., Liu, G.F., Shtykova, E.V., Xu, J.H., Li,
1343 L.F., Su, X.D., and Dong, Y.H. (2012). The crystal structure of the MPN domain
1344 from the COP9 signalosome subunit CSN6. FEBS Lett, *586*, 1147–1153.
1345 127. Zhou, C., Wee, S., Rhee, E., Naumann, M., Dubiel, W., and Wolf, D.A.
1346 (2003). Fission yeast COP9/signalosome suppresses cullin activity through
1347 recruitment of the deubiquitylating enzyme Ubp12p. Mol Cell, *11*, 927–938.
1348

1349 **Figure Legends:**

1350 **Fig. 1. CSN-5 interacts with FBFs.**

1351 (A) Schematic of adult *C. elegans* hermaphrodite gonad. Stem and progenitor cells
1352 (SPCs) expressing FBF proteins are highlighted in green. COP9 subunit CSN-5 is
1353 expressed throughout oogenic germline. (B) Interaction between CSN-5 and FBF-1/-2 is
1354 detected in a yeast two-hybrid assay with FBFs fused to Gal4 DNA-binding domain as
1355 baits and CSN-5 fused to Gal4 activation domain as prey. This experiment was
1356 performed in two replicates. (C) Western blot confirming expression of FBFs and CSN-5
1357 in yeast cultures. (D) GST pulldown assay detects a direct interaction between
1358 GST::CSN-5 and both His_6::FBF-1 and His_6::FBF-2. FBFs are detected by Western blot

1359 with anti-His. Total protein (representative image from FBF-2 pulldown) detected by
1360 stain-free chemistry, the position of GST::CSN-5 is marked with a black dot.

1361 **Fig. 2. Interaction between FBF RNA-binding domain and MPN domain of CSN-5**
1362 **is conserved in evolution.**

1363 (A) GST or GST::CSN-5 were tested for binding His_6::FBF-1^{RBD}, His_6::FBF-2^{RBD}, and
1364 His_6::FBF-$2^{N\text{-}term}$ constructs. Proteins are detected by Western blot with anti-His and
1365 anti-GST, the position of GST::CSN-5 (representative image from His_6::FBF-$2^{N\text{-}term}$
1366 pulldown) is marked with a black dot. (B) FBF-1/-2 and PUM1/2 truncation constructs.
1367 Grey: RNA-binding domain. Amino acid positions of the truncations are indicated above
1368 each construct. (C) GST::CSN-5 truncation constructs were tested for binding
1369 His_6::FBF-2. Proteins are detected by Western blot with anti-His and anti-GST, the
1370 positions of GST-tagged constructs are marked with a black dot. (D) CSN-5, CSN-6,
1371 and CSN5 truncation constructs. Brown: core MPN domain. C-terminal helices (purple
1372 ovals) that incorporate into the helical bundle of the COP9 signalosome (Lingaraju et al.,
1373 2014). Amino acid positions of the truncations are indicated above each construct. (E)
1374 GST pulldown of His_6::FBF-2 with GST::CSN-5^{MPN} and increasing concentrations of
1375 GST::CSN-6^{MPN} as detected by Western blot with anti-His. Total protein seen by
1376 Coomassie. See also Fig. S1. (F) GST pulldown of human homologs, GST::$CSN5^{MPN}$
1377 with His_6::$PUM1^{RBD}$ or His_6::$PUM2^{RBD}$, as detected by Western blot with anti-His. Total
1378 protein (representative image from His_6::$PUM2^{RBD}$ pulldown) detected by stain-free
1379 chemistry.

1380 **Fig. 3. FBF-2 interacts with CSN-5 *in vivo*.**

1381 (A) Confocal images of the distal germline SPC zones with PLA foci (yellow) and DAPI
1382 (blue). Germlines are outlined with dashed lines and vertical dotted lines indicate the
1383 beginning of the transition zone. Genotypes are indicated with their respective images.
1384 Scale bars: 10 μm. (B) The PLA density (number of PLA foci per μm^2) within the SPC
1385 zone was measured for germlines of each genetic background. Differences in PLA
1386 density for each protein was evaluated by one-way ANOVA with Tukey's post-test.
1387 Asterisks denote statistical significance (****, $p<0.0001$) where FBF-2 had significantly

more PLA foci than both FBF-1 and the control. Number of germlines scored (*N*) are indicated below the graph. Data is representative of 3 biological replicates and error bars denote SEM. All experiments were performed at 24°C.

Fig. 4. FBF-1/-2, but not PUF-3, protein levels are reduced in *csn(lf)* mutants.

(A) Western blot analysis of *3xv5::fbf-2(q932),* referred to here as wild type, and respective *3xv5::fbf-2(q932); csn(lf)* mutant worm lysate reveals reduced levels of FBF-1 (top panels) and 3xV5::FBF-2 (bottom panels). Tubulin is used as a loading control. Endogenous FBF-1 and epitope-tagged endogenous 3xV5::FBF-2 are detected by anti-FBF-1 and anti-V5. (B, C) Total FBF protein level of each *3xv5::fbf-2(q932); csn(lf)* mutant normalized to *3xv5::fbf-2(q932)*, referred to here as wild type. Differences in protein level were evaluated by one-way ANOVA with Tukey's post-test. Grey asterisks denote statistical significance compared to wild type and blue bracket and asterisk denote statistical significance comparing *csn-2(lf)* to *csn-5(lf)* (*, $p<0.05$; **, $p<0.01$; ***, $p<0.005$; ****, $p<0.0001$). Number of biological replicates (*N*) is indicated at the bottom of the graphs. Mean group values are shown as lines and error bars denote standard deviation. (D-K) Gonads of *csn(lf)* mutants are dissected and stained with (D-G) anti-FBF-1 (green) or (H-K) anti-V5 (green) and DAPI (blue) to visualize protein levels of FBF-1/-2. The individual FBF (green) and DAPI (greyscale) channels are also shown for better contrast. (L, M) Distal germlines dissected from adult *3xv5::puf-3* and *csn-5(lf) 3xv5::puf-3* dissected and stained with anti-V5 (green) and DAPI (grey). Germlines are outlined with dashed lines and vertical dotted lines indicate border of the SPC zone. Scale bars: 10 µm. (N) Quantification of SPC expression of 3xV5::PUF-3 protein. Maximum PUF-3 levels in each germline are scaled to average levels in the *3xv5::puf-3* strain. Differences in maximum protein level were evaluated by Student's t-test. Grey asterisks denote statistical significance (****, $p<0.0001$). Number of germlines scored (*N*) is indicated at the bottom of the graphs. Mean group values are shown as lines and error bars denote standard deviation. Data reflect three biological replicates.

Fig. 5. COP9 subunit mutants have reduced number of stem cells but sustain proliferation and meiotic entry.

1417 (Ai-iv) Distal germlines dissected from adult *3xv5::fbf-2(q932)*, referred to as wild type,
1418 and respective *3xv5::fbf-2(q932); csn(lf)* mutants were stained with anti-REC-8 (green)
1419 to visualize SPC zone. Germlines are outlined with dashed lines and vertical dotted
1420 lines indicate the SPC zone boundary. Scale bars: 10 μm. (B) Quantification of SPCs in
1421 wild type and *csn(lf)* mutants. Differences in number of SPCs was evaluated by one-
1422 way ANOVA with Tukey's post-test. Grey asterisks denote statistical significance
1423 compared to wild type (****, $p<0.0001$) and blue asterisks denote statistical significance
1424 compared to *csn-2(lf)* (**, $p<0.01$). Number of germlines scored (*N*) are indicated at the
1425 bottom of the graph. Stem cell quantification reflects six biological replicates of wild type
1426 and three biological replicates for each *csn(lf)* mutant. (Ci-iii) Distal germlines dissected
1427 from adult *3xv5::fbf-2(q932)*, referred to as wild type, and respective *3xv5::fbf-2(q932);*
1428 *csn(lf)* mutants were stained for EdU and pH3 to visualize cells in S-phase and identify
1429 mitotically dividing cells, respectively. Germlines are outlined with dashed lines. Scale
1430 bars: 10 μm. (D) Germlines were scored for the presence of EdU incorporation, pH3(+)
1431 cells, both, or neither. Number of germlines scored (*N*) are indicated at the top of each
1432 column. Data are plotted in aggregate and reflect two biological replicates. (E-G) Distal
1433 germlines from adult *3xv5::fbf-2(q932)*, referred to as wild type, and respective
1434 *3xv5::fbf-2(q932); csn(lf)* mutants dissected and stained for EdU and REC-8 to visualize
1435 cells in S-phase and the SPC zone, respectively. Arrows indicate EdU(+)/REC-8(-) cells
1436 entering meiosis. Corresponding percent of germlines entering meiosis with number of
1437 germlines scored (*N*) indicated in overlay panels (iii), data reflect two biological
1438 replicates. Germlines are outlined with dashed lines and vertical dotted lines indicate
1439 the SPC boundary. Scale bars: 10 μm.

1440 **Fig. 6. Mutations in COP9 subunits disrupt oogenesis.**

1441 (Ai-iv) Gonads of adult *3xv5::fbf-2(q932)*, referred to as wild type, and respective
1442 *3xv5::fbf-2(q932); csn(lf)* mutants indicated in each panel dissected and stained for DNA
1443 with DAPI. Arrows indicate gametes. Germlines are outlined with dashed lines. Scale
1444 bars: 10 μm. (B) Gametogenesis in wild type and *csn(lf)* mutants. Number of germlines
1445 scored (*N*) are indicated at the top of each column. Data are plotted in aggregate and
1446 reflect six biological replicates of wild type, four replicates of *csn-6(lf)*, three replicates of

1447 each *csn-2(lf)* and *csn-5(lf)*, and two replicates of *csn-2(lf); fbf-1(lf)*. (C) Female fate of
1448 *csn-6(lf)* is partially restored by an extra copy of *csn-5* gene in *3xflag::csn-5; csn-6(lf)*
1449 strain. Number of germlines scored (*N*) are indicated at the top of the graph. Data are
1450 plotted in aggregate and reflect three biological replicates. (D, E) Gonads of adult
1451 *3xv5::puf-3* and *csn-5(lf) 3xv5::puf-3* mutant indicated in each panel dissected and
1452 stained for DNA with DAPI (cyan/grey), V5::PUF-3 with anti-V5 (D, red), or sperm with
1453 anti-MSP (E, green). Arrows indicate gametes. Germlines are outlined with dashed
1454 lines. Scale bars: 10 μm.

1455 **Fig. 7. *csn-5(lf)* destabilizes FBF proteins.**

1456 (A, C) FBF protein levels after treatment with a control RNAi and *pbs-6(RNAi)* in *rrf-1(lf);*
1457 *3xv5::fbf-2(q932)*, referred to as *rrf-1(pk1417)* here, and *rrf-1(lf); 3xv5::fbf-2(q932); csn-*
1458 *5(lf)*, referred to as *rrf-1(pk1417); csn-5(ok1064)*. (A) Endogenous FBF-1 and (C)
1459 epitope-tagged endogenous 3xV5::FBF-2 are detected by anti-FBF-1 and anti-V5.
1460 Tubulin is used as a loading control. (B, D) Total FBF protein levels of *csn-5(lf)*
1461 normalized to wild type control RNAi. Control RNAi data points for each genetic
1462 background are shown as circles and *pbs-6(RNAi)* is shown as the triangles. Difference
1463 in FBF protein level was evaluated by one-way ANOVA with Sidak's post-test. Red
1464 brackets with asterisks denote statistical significance comparing *csn-5(lf)* control RNAi
1465 to *csn-5(lf) pbs-6(RNAi)* (*, $p<0.05$; **, $p<0.01$), ns denotes not significant. Number of
1466 biological replicates (*N*) is indicated below the graph, mean value is indicated as a line,
1467 and error bars denote standard deviation. (E) Steady-state levels of transcripts indicated
1468 on the X-axis are quantified by RT-qPCR and normalized to reference gene *act-1*; *unc-*
1469 *54* is a control. Differences in relative mRNA abundance of *fbf-1/-2* were evaluated by
1470 one-way ANOVA with Dunnett's post-test. Asterisks denote statistical significance
1471 compared to wild type control RNAi (**, $p<0.01$; ***, $p<0.005$; ****, $p<0.0001$). The data
1472 reflect four biological replicates of control RNAi for *rrf-1(lf)* and *rrf-1(lf); csn-5(ok1064),*
1473 three replicates of *rrf-1(lf); pbs-6(RNAi)*, and two replicates of *rrf-1(lf); csn-5(ok1064);*
1474 *pbs-6(RNAi)*. Mean values are plotted as lines with error bars representing standard
1475 deviation.

1476 **Fig. 8. *ned-8(RNAi)* rescues phenotypes seen in *csn-5(lf)*.**

1477 (A, B) Maximum intensity of FBF-1 (A) and FBF-2 (B) immunostaining of *3xv5::fbf-*
1478 *2(q932)*, referred to here as wild type, and *3xv5::fbf-2; csn-5(lf)*, referred to here as *csn-*
1479 *5(lf)* treated with control or *ned-8(RNAi)*. Endogenous FBF-1 and epitope-tagged
1480 endogenous 3xV5::FBF-2 detected by anti-FBF-1 and anti-V5. Maximal FBF protein
1481 intensity in each germline was normalized to the average of wild type control RNAi.
1482 Differences in protein level were evaluated by one-way ANOVA with Sidak's post-test,
1483 ns denotes not significant, red asterisks denote statistical significance (****, $p<0.0001$).
1484 Number of germlines scored (*N*) is indicated at the bottom of the graphs. Mean group
1485 values are shown as lines and error bars denote standard deviation. The data reflect
1486 three biological replicates. (C-F) Gonads of wild type and *csn-5(lf)* mutant are dissected
1487 and stained with anti-FBF-1 (red) or anti-V5 (green) and DAPI (not shown) to visualize
1488 protein levels of FBF-1/-2. (G) Quantification of SPCs in wild type and *csn(lf)* mutants
1489 with *ned-8(RNAi)*. Differences in number of SPCs were evaluated by one-way ANOVA
1490 with Sidak's post-test. ns denotes not significant and red asterisks denote statistical
1491 significance (****, $p<0.0001$). Number of germlines scored (*N*) are indicated at the
1492 bottom of the graph. Stem cell quantification reflects four biological replicates of *csn-*
1493 *5(lf)* control RNAi and three biological replicates of wild type control RNAi, wild type
1494 *ned-8(RNAi)*, and *csn-5(lf) ned-8(RNAi*). (H) Gametogenesis in *ned-8(RNAi)* treated
1495 wild type and *csn-5(lf)* mutant. Number of germlines scored (*N*) are indicated at the top
1496 of each column. Data are plotted in aggregate and reflect three biological replicates.

1497 **Fig. 9. Model of CSN-5 stabilizing FBFs.**

1498 (A) CSN-5 promotes the stability of FBFs both in the context of COP9 signalosome and
1499 independent of COP9, thereby allowing FBFs proteins to maintain the SPC zone and
1500 enable the switch from spermatogenesis to oogenesis. (B) Intrinsically unstable FBF
1501 proteins are readily degraded by the proteasome resulting in a germline with fewer
1502 SPCs and no female gametes in the absence of CSN-5.

1503 **Fig. S1. RNA-independent FBF-2 interaction with CSN-5 and CSN-6.**

1504 (A) GST pulldown assay of His_6::FBF-2 with GST::CSN-5^{MPN} or (B) GST::CSN-6^{MPN} with
1505 or without RNase A treatment. FBF-2 protein is detected by Western blot with anti-His.
1506 Total protein seen by Coomassie.

1507 **Fig. S2. Relative *fbf-2* transcript abundance is reduced in *csn(lf)* mutants.**

1508 Steady-state levels of transcripts indicated on the X-axis in *3xv5::fbf-2(q932)*, referred to
1509 here as wild type, and *3xv5::fbf-2(q932); csn(lf)* mutants are quantified by RT-qPCR and
1510 normalized to reference gene *act-1*. *unc-54* is a control. Differences in relative mRNA
1511 abundance of *fbf-1/-2* was evaluated by one-way ANOVA with Dunnett's post-test. Grey
1512 asterisks denote statistical significance compared to wild type (****, $p<0.0001$). Data are
1513 representative of five biological replicates of wild type, four replicates of both *csn-2(lf)*
1514 and *csn-6(lf)*, and three biological replicates of *csn-5(lf)*. Data are plotted as mean
1515 values with error bars representing standard deviation.

1516 **Fig. S3. *csn-5(lf)* functions in the same pathway as *fbfs* in SPC maintenance.**

1517 Quantification of SPCs (by anti-REC-8 staining) after treatment with a control RNAi
1518 (circles) and *fbf(RNAi)* (triangles) in *3xv5::fbf-2(q932); csn-5(lf)/nT1*, referred to here as
1519 *csn-5(ok1064)/nT1* (grey), and *3xv5::fbf-2(q932); csn-5(lf)* referred to as *csn-5(ok1064)*
1520 (red). Differences in number of SPCs were evaluated by one-way ANOVA with Sidak's
1521 post-test, ns denotes not significant. Number of germlines scored (*N*) are indicated at
1522 the bottom of the graph. Data reflects two biological replicates.

1523 **Fig. S4. FBF levels are similar in hermaphrodites and males; CSN-5 levels are**
1524 **reduced in *csn-6(lf)*, and catalytically dead CSN-5 maintains binding to FBF-2 *in***
1525 ***vitro*.**

1526 (Ai, iii) Western blot analysis comparing worm lysate of hermaphrodites to males in *rrf-*
1527 *1(pk1417); 3xv5::fbf-2(q932); him-8(tm611)* mutants. Endogenous FBF-1 and epitope-
1528 tagged endogenous 3xV5::FBF-2 are detected by anti-FBF-1 and anti-V5. Tubulin is
1529 used as a loading control. (Aii, iv) Total protein in males was normalized to
1530 hermaphrodites. Differences in protein level were evaluated by Student's t-test, ns
1531 denotes not significant. The data reflect four biological replicates for FBF-2 and three
1532 biological replicates for FBF-1. Mean group values are shown as lines and error bars
1533 denote standard deviation. (Bi) 3xFLAG::CSN-5 protein levels in *3xflag::csn-5* and
1534 *3xflag::csn-5; csn-6(ok1604)* animals detected by Western blot with anti-FLAG. Tubulin
1535 is used as a loading control. (Bii) Relative level of 3xFLAG::CSN-5 protein in *csn-6(lf)*

1536 was normalized to the wild type. Difference in protein level was evaluated by Student's
1537 t-test. Asterisks denote statistical significance (***, $p<0.005$). The data reflect six
1538 biological replicates, is represented as average values, and error bars denote standard
1539 deviation. (C) GST pulldown of His_6::FBF-2 with GST::CSN-5(D152N). Protein
1540 constructs are detected by Western blot with anti-His and anti-GST, the positions of
1541 GST::CSN-5 constructs are marked by a black dot.

1542 **Fig. S5. Oogenesis is restored in *rrf-1(lf); csn-5(lf)* mutant backgrounds.**

1543 Gametogenesis in *pbs-6(RNAi)*-treated *rrf-1(pk1417); fbf-2(q932)* and *rrf-1(pk1417); fbf-*
1544 *2(q932); csn-5(ok1064)* mutants. Number of germlines scored (*N*) are indicated at the
1545 top of each column. Data are plotted in aggregate and reflect two biological replicates.

1546 **Fig. S6. *csn-2(ok1288)* allele used in this study.**

1547 (A) Schematic diagram of *csn-2(ok1288)* locus with exons pictured as black rectangles,
1548 introns as black lines, and the UTRs as grey rectangles. The 1680 nucleotide *ok1288*
1549 deletion (red) results in the removal of most of intron 3, exon 4, and most of intron 4.
1550 The spliced transcript results in a frameshift at amino acid 238 and a premature stop
1551 codon. (B) The schematic of full-length CSN-2 protein compared to CSN-2(ok1288)
1552 shows the *ok1288* deletion removing three C-terminal PCI repeats (squares), the
1553 winged-helix (WH) subdomain, and the C-terminal helix (oval). Domains of CSN-2 are
1554 delineated by homology with human CSN2 from a previous report (Lingaraju et al.,
1555 2014).-

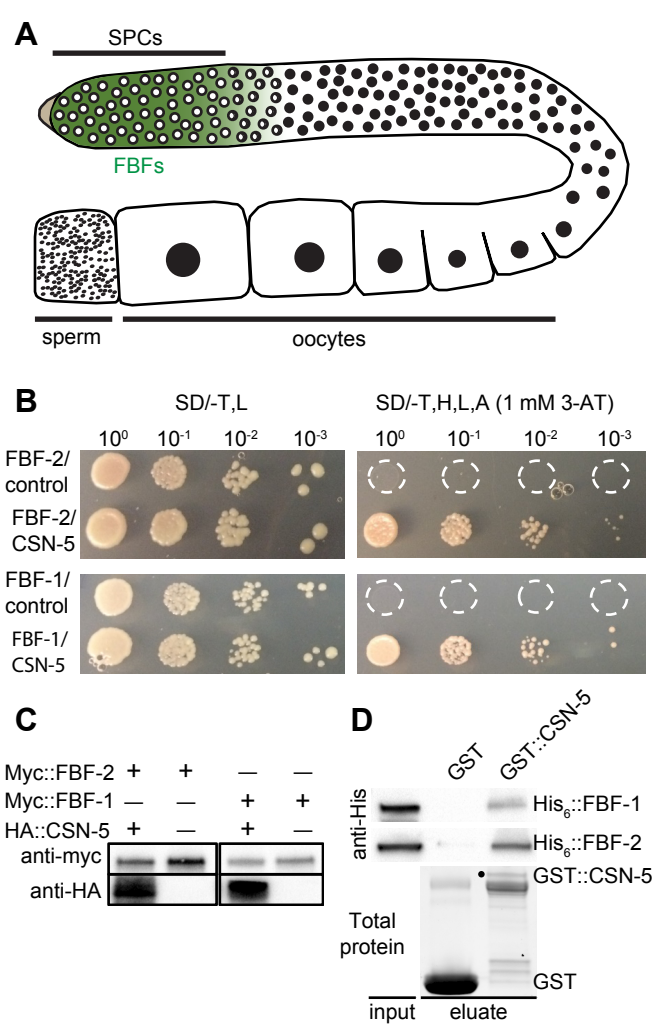
A
SPCs
FBFs
sperm
oocytes
B
SD/-T,L
SD/-T,H,L,A (1 mM 3-AT)
10^0
10^-1
10^-2
10^-3
FBF-2/ control
FBF-2/ CSN-5
FBF-1/ control
FBF-1/ CSN-5
C
Myc::FBF-2 + + — —
Myc::FBF-1 — — + +
HA::CSN-5 + — + —
anti-myc
anti-HA
D
GST
GST::CSN-5
anti-His
His6::FBF-1
His6::FBF-2
GST::CSN-5
Total protein
GST
input
eluate

Figure 1.

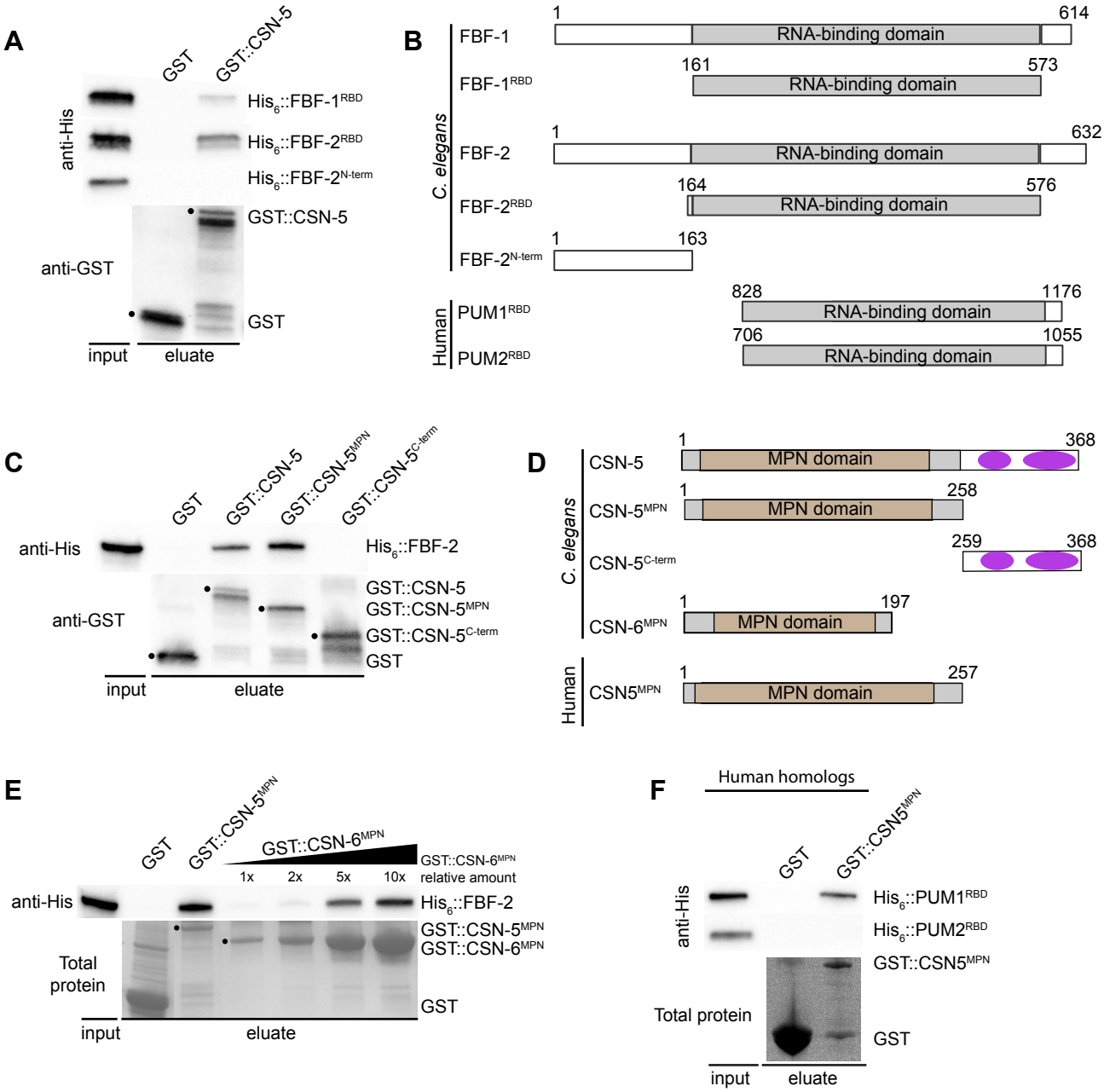
A
GST
GST::CSN-5
anti-His
His6::FBF-1RBD
His6::FBF-2RBD
His6::FBF-2N-term
GST::CSN-5
anti-GST
GST
input
eluate
B
C. elegans
FBF-1
1
614
RNA-binding domain
FBF-1RBD
161
573
RNA-binding domain
FBF-2
1
632
RNA-binding domain
FBF-2RBD
164
576
RNA-binding domain
FBF-2N-term
1
163
Human
PUM1RBD
828
1176
RNA-binding domain
PUM2RBD
706
1055
RNA-binding domain
C
GST
GST::CSN-5
GST::CSN-5MPN
GST::CSN-5C-term
anti-His
His6::FBF-2
anti-GST
GST::CSN-5
GST::CSN-5MPN
GST::CSN-5C-term
GST
input
eluate
D
C. elegans
CSN-5
1
368
MPN domain
CSN-5MPN
1
258
MPN domain
CSN-5C-term
259
368
CSN-6MPN
1
197
MPN domain
Human
CSN5MPN
1
257
MPN domain
E
GST
GST::CSN-5MPN
GST::CSN-6MPN
1x
2x
5x
10x
GST::CSN-6MPN relative amount
anti-His
His6::FBF-2
Total protein
GST::CSN-5MPN
GST::CSN-6MPN
GST
input
eluate
F
Human homologs
GST
GST::CSN5MPN
anti-His
His6::PUM1RBD
His6::PUM2RBD
GST::CSN5MPN
Total protein
GST
input
eluate

Figure 2.

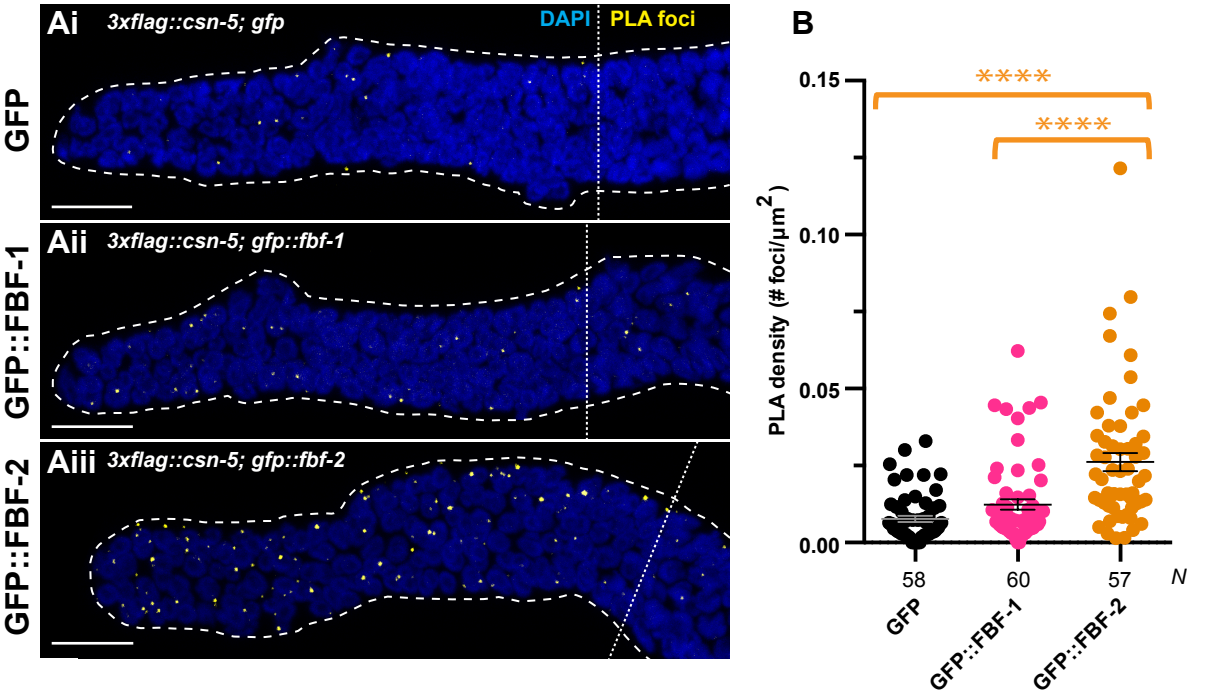
Ai
3xflag::csn-5; gfp
DAPI
PLA foci
GFP
Aii
3xflag::csn-5; gfp::fbf-1
GFP::FBF-1
Aiii
3xflag::csn-5; gfp::fbf-2
GFP::FBF-2
B
PLA density (# foci/µm2)
0.15
0.10
0.05
0.00
****
****
58
60
57
N
GFP
GFP::FBF-1
GFP::FBF-2

Figure 3.

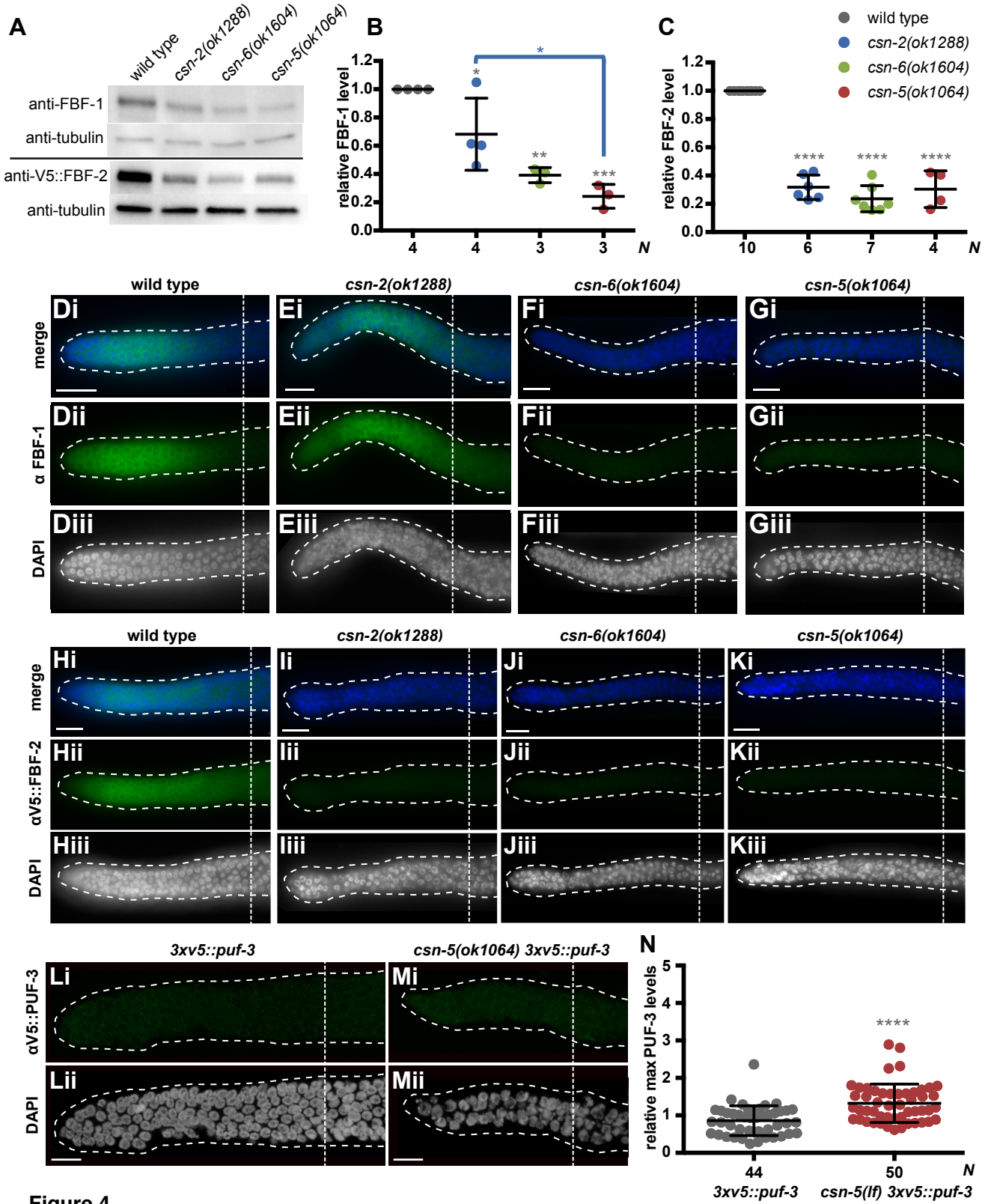
A
wild type
csn-2(ok1288)
csn-6(ok1604)
csn-5(ok1064)
anti-FBF-1
anti-tubulin
anti-V5::FBF-2
anti-tubulin
B
relative FBF-1 level
N
C
wild type
csn-2(ok1288)
csn-6(ok1604)
csn-5(ok1064)
relative FBF-2 level
N
wild type
csn-2(ok1288)
csn-6(ok1604)
csn-5(ok1064)
merge
α FBF-1
DAPI
αV5::FBF-2
3xv5::puf-3
csn-5(ok1064) 3xv5::puf-3
αV5::PUF-3
N
relative max PUF-3 levels
3xv5::puf-3
csn-5(lf) 3xv5::puf-3

Figure 4.

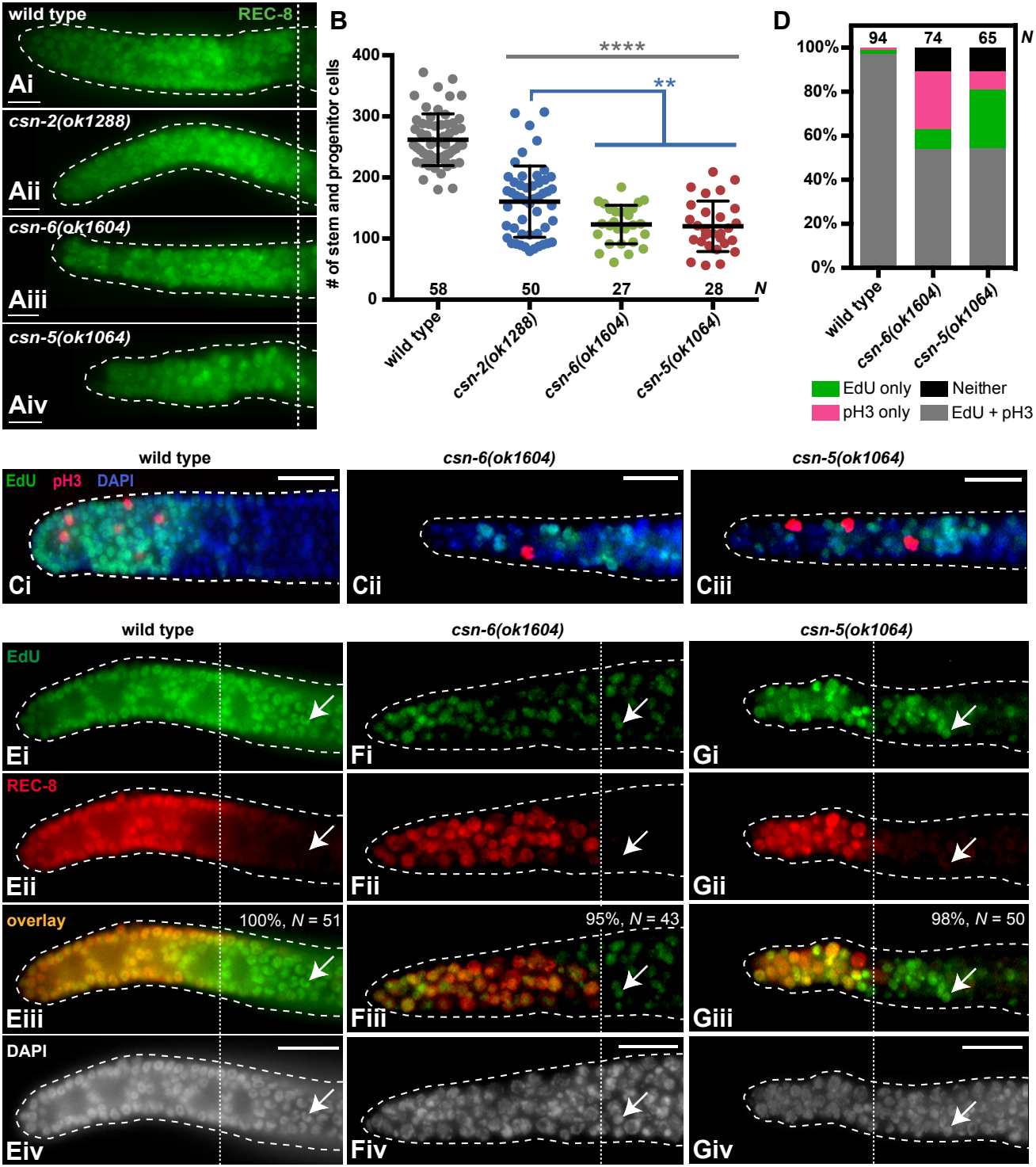
wild type
REC-8
Ai
csn-2(ok1288)
Aii
csn-6(ok1604)
Aiii
csn-5(ok1064)
Aiv
B
# of stem and progenitor cells
400
300
200
100
0
****
**
58
50
27
28
N
wild type
csn-2(ok1288)
csn-6(ok1604)
csn-5(ok1064)
D
94
74
65
N
100%
80%
60%
40%
20%
0%
wild type
csn-6(ok1604)
csn-5(ok1064)
EdU only
Neither
pH3 only
EdU + pH3
wild type
csn-6(ok1604)
csn-5(ok1064)
EdU
pH3
DAPI
Ci
Cii
Ciii
wild type
csn-6(ok1604)
csn-5(ok1064)
EdU
Ei
Fi
Gi
REC-8
Eii
Fii
Gii
overlay
100%, N = 51
95%, N = 43
98%, N = 50
Eiii
Fiii
Giii
DAPI
Eiv
Fiv
Giv

Figure 5.

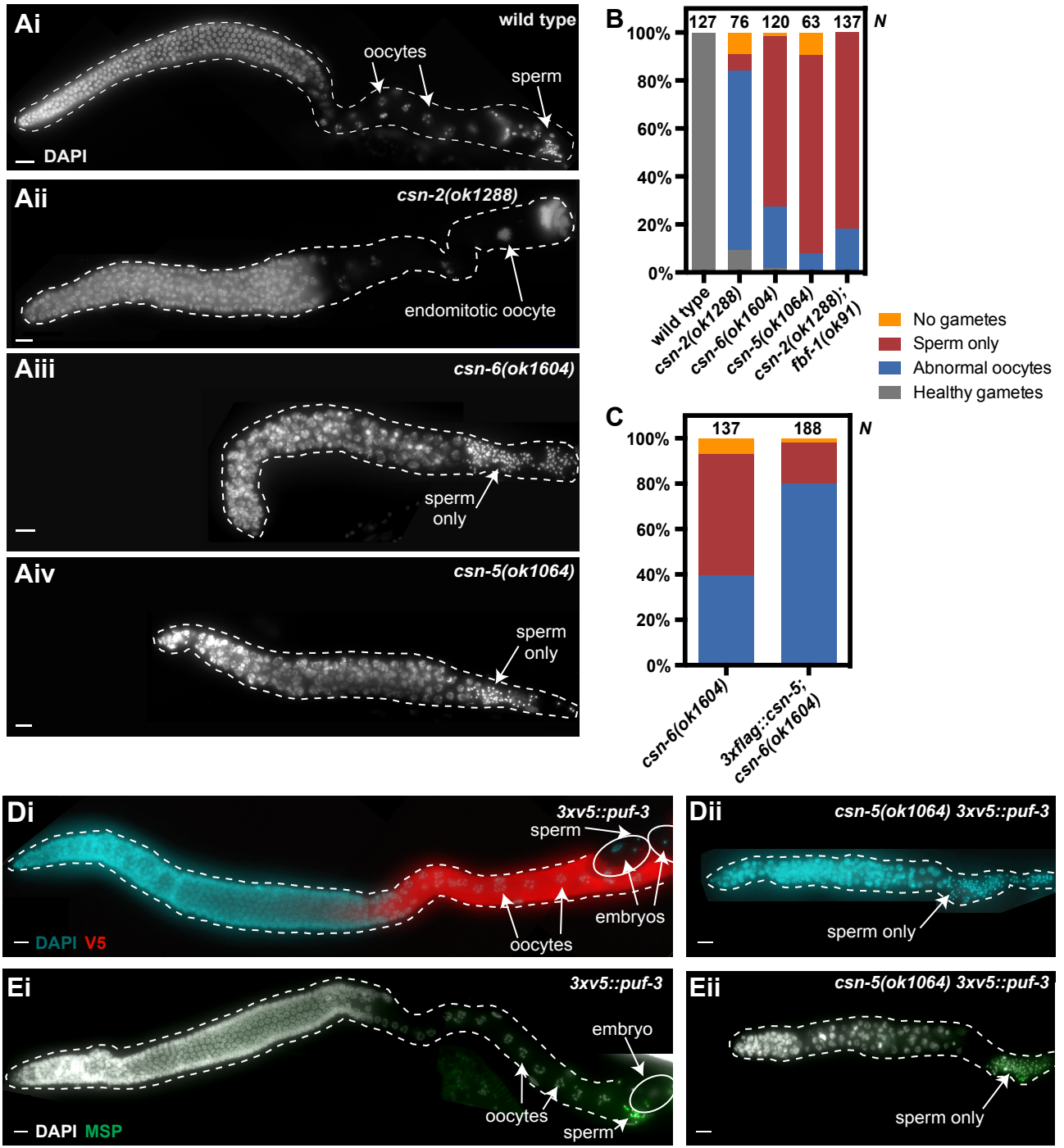
Ai
wild type
oocytes
sperm
DAPI
Aii
csn-2(ok1288)
endomitotic oocyte
Aiii
csn-6(ok1604)
sperm only
Aiv
csn-5(ok1064)
sperm only
B
127
76
120
63
137
N
100%
80%
60%
40%
20%
0%
wild type
csn-2(ok1288)
csn-6(ok1604)
csn-5(ok1064)
csn-2(ok1288); fbf-1(ok91)
No gametes
Sperm only
Abnormal oocytes
Healthy gametes
C
137
188
N
100%
80%
60%
40%
20%
0%
csn-6(ok1604)
3xflag::csn-5; csn-6(ok1604)
Di
3xv5::puf-3
sperm
embryos
oocytes
DAPI V5
Dii
csn-5(ok1064) 3xv5::puf-3
sperm only
Ei
3xv5::puf-3
embryo
oocytes
sperm
DAPI MSP
Eii
csn-5(ok1064) 3xv5::puf-3
sperm only

Figure 6.

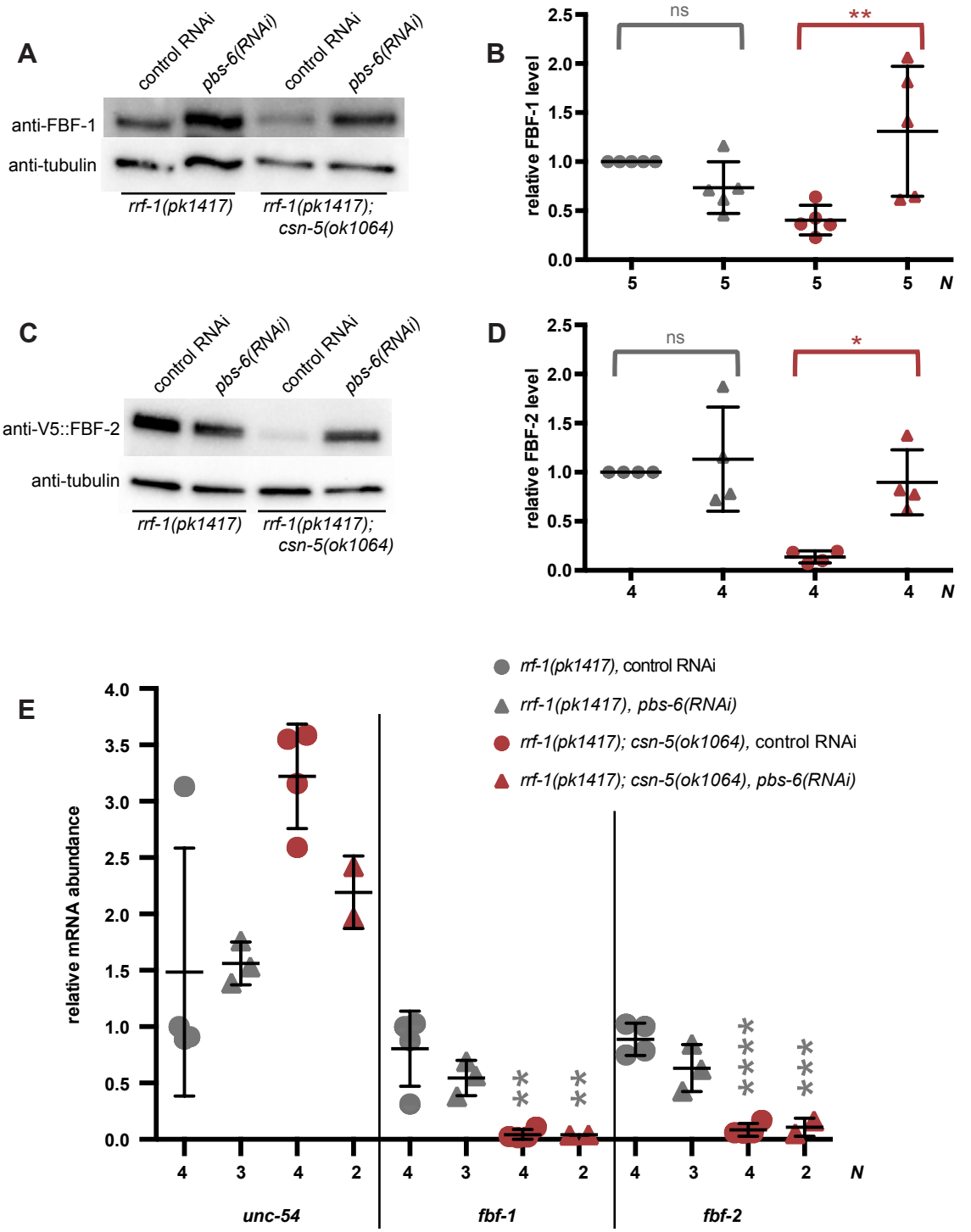
A
control RNAi
pbs-6(RNAi)
control RNAi
pbs-6(RNAi)
anti-FBF-1
anti-tubulin
rrf-1(pk1417)
rrf-1(pk1417); csn-5(ok1064)
B
relative FBF-1 level
ns
**
N
C
control RNAi
pbs-6(RNAi)
control RNAi
pbs-6(RNAi)
anti-V5::FBF-2
anti-tubulin
rrf-1(pk1417)
rrf-1(pk1417); csn-5(ok1064)
D
relative FBF-2 level
ns
*
N
E
relative mRNA abundance
rrf-1(pk1417), control RNAi
rrf-1(pk1417), pbs-6(RNAi)
rrf-1(pk1417); csn-5(ok1064), control RNAi
rrf-1(pk1417); csn-5(ok1064), pbs-6(RNAi)
unc-54
fbf-1
fbf-2
N

Figure 7.

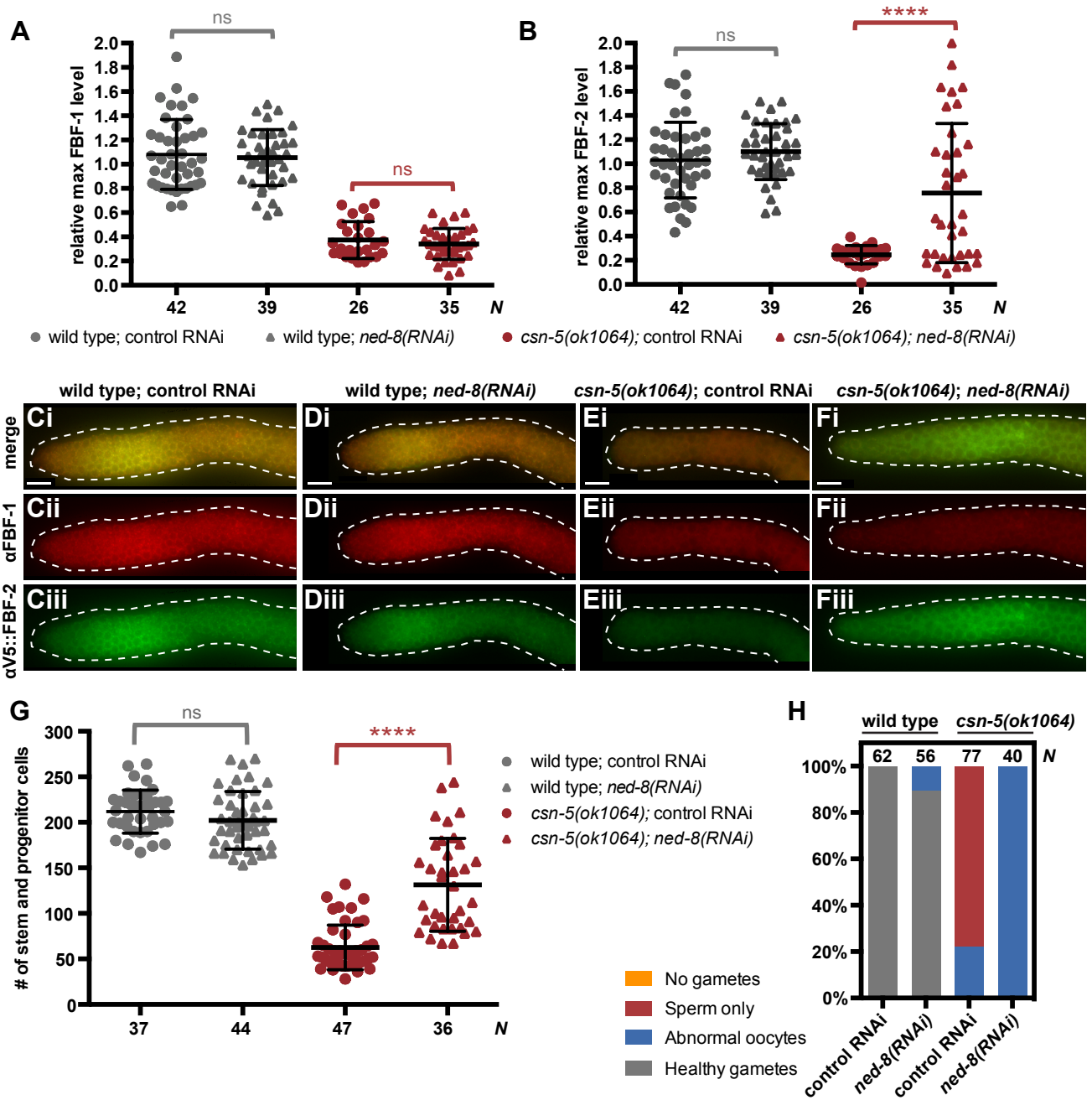
A
relative max FBF-1 level
ns
ns
42
39
26
35
N
B
relative max FBF-2 level
ns
****
42
39
26
35
N
wild type; control RNAi
wild type; ned-8(RNAi)
csn-5(ok1064); control RNAi
csn-5(ok1064); ned-8(RNAi)
wild type; control RNAi
wild type; ned-8(RNAi)
csn-5(ok1064); control RNAi
csn-5(ok1064); ned-8(RNAi)
merge
αFBF-1
αV5::FBF-2
Ci
Di
Ei
Fi
Cii
Dii
Eii
Fii
Ciii
Diii
Eiii
Fiii
G
# of stem and progenitor cells
ns
****
37
44
47
36
N
wild type; control RNAi
wild type; ned-8(RNAi)
csn-5(ok1064); control RNAi
csn-5(ok1064); ned-8(RNAi)
No gametes
Sperm only
Abnormal oocytes
Healthy gametes
H
wild type
csn-5(ok1064)
62
56
77
40
N
control RNAi
ned-8(RNAi)
control RNAi
ned-8(RNAi)

Figure 8.

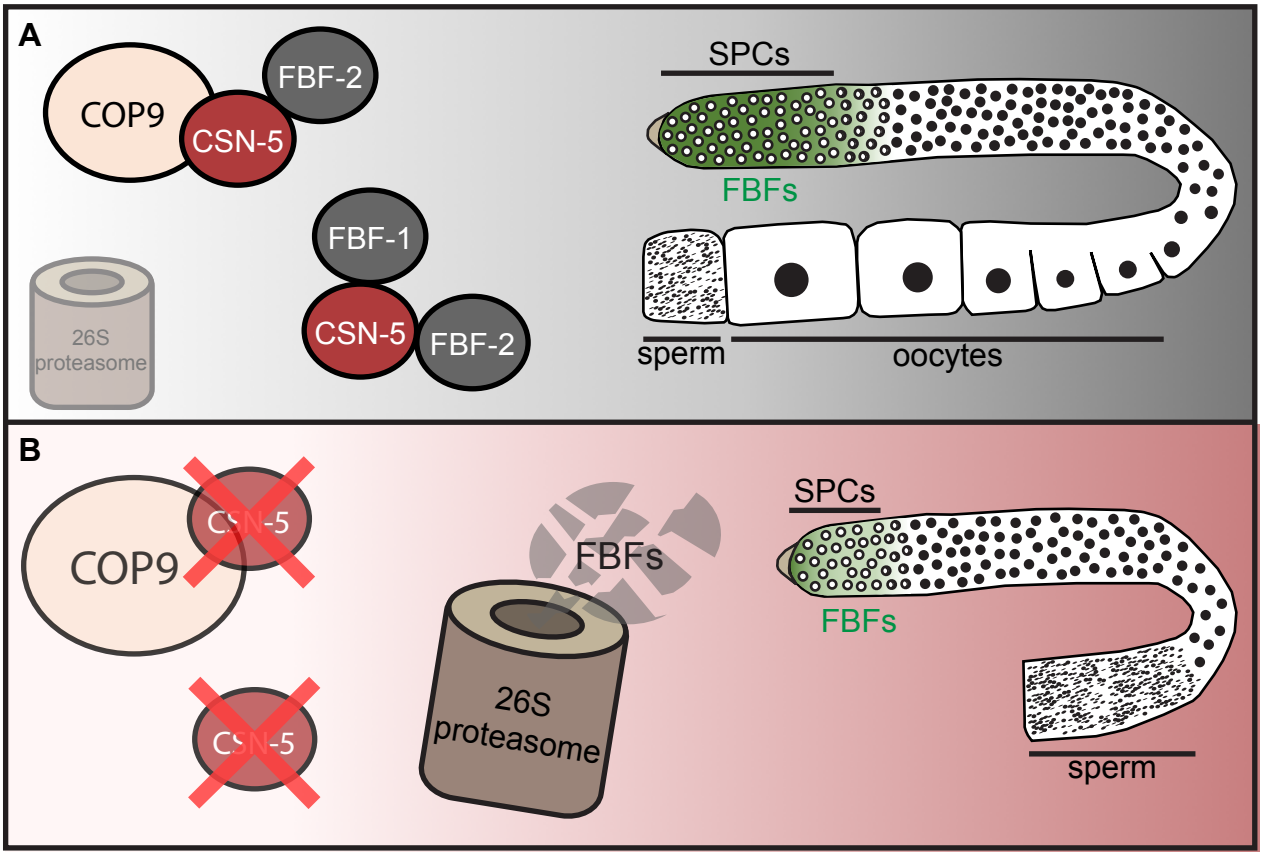
A
COP9
CSN-5
FBF-2
26S
proteasome
FBF-1
CSN-5
FBF-2
SPCs
FBFs
sperm
oocytes
B
COP9
CSN-5
CSN-5
FBFs
26S
proteasome
SPCs
FBFs
sperm

Figure 9.